Quantitative J correlation methods for the accurate measurement of $^{13}C'$-$^{13}C^\alpha$ dipolar couplings in proteins

Christopher P. Jaroniec , Tobias S. Ulmer & Ad Bax
Laboratory of Chemical Physics, National Institute of Diabetes and Digestive and Kidney Diseases, National Institutes of Health, Bethesda, MD 20892-0520, U.S.A.

Abstract

Methods are described for the precise and accurate measurement of one-bond dipolar $^{13}C'$-$^{13}C^\alpha$ couplings in weakly aligned proteins. The experiments are based on the principle of quantitative J correlation, where $^1J_{C'C^\alpha}$ (or $^1J_{C'C^\alpha} + {}^1D_{C'C^\alpha}$) is measured from the relative intensity of two interleaved 3D TROSY-HN(CO)CA or 3D TROSY-HNCO spectra recorded with dephasing intervals of zero (reference spectrum) and $\sim 3/(2^1J_{C'C^\alpha})$ (attenuated spectrum). In analogy to other quantitative J correlation techniques, the random error in the measured $^1J_{C'C^\alpha}$ value is inversely proportional to the signal-to-noise ratio in the reference spectrum. It is shown that for weakly aligned proteins, with the magnitude of the alignment tensor of $D_a^{NH} \leq 10$–15 Hz, the systematic errors are typically negligible. The methods are demonstrated for the third IgG-binding domain of protein G (GB3) and α-synuclein in complex with a detergent micelle, where errors in $^1D_{C'C^\alpha}$ of less than 0.1 Hz and ca. 0.2 Hz, respectively, are estimated. Remarkably, the dipolar couplings determined for GB3 are in even better agreement with the recently refined 1.1-Å X-ray structure than the input $^{13}C'$-$^{13}C^\alpha$ couplings used for the refinement.

Introduction

Dipolar couplings are sensitive probes of local and long-range molecular geometry and can considerably improve the accuracy of macromolecular structures determined by NMR techniques (Tjandra et al., 1997; Clore et al., 1999; Prestegard et al., 2000; Bax et al., 2001). These interactions can be detected in high-resolution solution-state NMR spectra of macromolecules having a sufficiently large magnetic susceptibility anisotropy, either intrinsic or introduced by chelating paramagnetic ions (Tolman et al., 1995; Tjandra et al., 1997; Ma and Opella, 2000), or molecules dissolved in slightly anisotropic media (Tjandra and Bax, 1997). Commonly used anisotropic media include dilute liquid crystalline phases, such as bicelles (Tjandra and Bax, 1997), filamentous phage particles (Clore et al., 1998b; Hansen et al., 1998) and mixtures of alkyl poly(ethylene glycol) and hexanol (Rückert and Otting, 2000), and compressed or stretched polyacrylamide gels (Sass et al., 2000; Tycko et al., 2000; Chou

et al., 2001). One-bond dipolar couplings involving the protein backbone atoms have a simple dependence on the fixed internuclear distance and can be used to relate directly the orientations of the corresponding bond vectors relative to the molecular alignment tensor. Consequently, accurate measurements of these couplings are of particular importance for the reliable characterization of the alignment tensor parameters in the absence of structural information (Clore et al., 1998a; Bryce and Bax, 2004), identification (Annila et al., 1999) and *de novo* determination (Delaglio et al., 2000) of protein backbone folds, and structure refinement (Tjandra et al., 1997; Clore et al., 1999; Meiler et al., 2000; Prestegard et al., 2000; Bax et al., 2001).

The present work deals with the measurement of backbone $^{13}C'$-$^{13}C^\alpha$ J and dipolar couplings in weakly aligned proteins, $^1J_{C'C^\alpha}$ and $^1D_{C'C^\alpha}$, respectively. Throughout the remainder of the discussion $^1J_{C'C^\alpha}$ will be used to denote *either* the one-bond $^{13}C'$-$^{13}C^\alpha$ J coupling in the isotropic phase *or* $^1J_{C'C^\alpha} + {}^1D_{C'C^\alpha}$

in the aligned phase, unless explicitly indicated otherwise. Because the dipolar coupling is directly proportional to the gyromagnetic ratios of the coupled spins and inversely proportional to the cube of the internuclear distance, $^1D_{C'C^\alpha}$ is inherently five times smaller than $^1D_{NH}$ (Bax et al., 2001), resulting in typical values of $|^1D_{C'C^\alpha}| \leq 5$ Hz for weakly aligned proteins. Due to its small magnitude the precise and accurate measurement of $^1D_{C'C^\alpha}$ is essential to its utility in protein structure determination. Several methods have been proposed for the measurement of $^1D_{C'C^\alpha}$ from the difference in $^1J_{C'C^\alpha}$ splittings obtained in isotropic and aligned phases. The simplest and most widely used approach involves the acquisition of a 3D HNCO spectrum (Grzesiek and Bax, 1992), with the C^α decoupling pulse during the C' evolution period omitted. This experiment has been extended to its transverse relaxation optimized (TROSY) version (Salzmann et al., 1999) and successfully applied to $^2H,^{13}C,^{15}N$-labeled proteins in the 30–40 kDa molecular weight range (Yang et al., 1999). Since each cross-peak in a $^{13}C^\alpha$-coupled HNCO spectrum gives rise to a $^{13}C'$-$\{^{13}C^\alpha\}$ doublet in the $^{13}C'$ dimension, in larger proteins some overlap can be expected between $^{13}C^\alpha = |\alpha\rangle$ and $^{13}C^\alpha = |\beta\rangle$ multiplet components belonging to different cross-peaks, which prohibits the accurate measurement of $^1J_{C'C^\alpha}$ for the residues involved. This problem has recently been addressed by methods that incorporate spin-state selection techniques (Sørensen et al., 1997; Ottiger et al., 1998) to display the $^{13}C^\alpha = |\alpha\rangle$ and $^{13}C^\alpha = |\beta\rangle$ multiplet components in separate spectra (Permi et al., 2000). In addition the $^{13}C'$ transverse relaxation rate, dominated by its large chemical shift anisotropy, increases significantly at higher magnetic field strengths (the $^{13}C'$ transverse relaxation rate at 800 MHz ^1H frequency increases by more than 50% over its 600 MHz value). This limits somewhat the full realization of the advantage of high fields in HNCO-based experiments for measuring $^{13}C'$-$^{13}C^\alpha$ dipolar couplings, since the uncertainty in the measurement of $^1J_{C'C^\alpha}$ from the frequency difference of two doublet components is directly proportional to the $^{13}C'$ linewidth (Kontaxis et al., 2000; Bax et al., 2001). By comparison, the $^{13}C^\alpha$ transverse relaxation rate in $^2H,^{13}C,^{15}N$-labeled proteins in the presence of ^2H decoupling is governed primarily by the one-bond ^2H-^{13}C dipolar interaction, and is roughly an order of magnitude smaller than the $^{13}C^\alpha$ relaxation rate in protonated systems (Grzesiek et al., 1993). Such favorable relaxation properties, exemplified by an average $^{13}C^\alpha$ T_2 value of ~130 ms

reported for a 70% $^2H,^{13}C,^{15}N$-labeled 37 kDa protein complex (Yamazaki et al., 1994), can be exploited for measuring $^1J_{C'C^\alpha}$ in high molecular weight proteins at high magnetic field strengths.

Here we describe simple methods for the precise and accurate measurement of $^1D_{C'C^\alpha}$ in weakly aligned proteins with high resolution and sensitivity. The experiments employ the principle of quantitative J correlation (Bax et al., 1994), where the value of $^1J_{C'C^\alpha}$ is obtained from the amplitude ratio of resonances in two three-dimensional spectra. The methods are designed to address the problems related to the extraction of the coupling magnitude from the frequency difference of two doublet components. In addition, one of the proposed experiments exploits the favorable relaxation properties of $^{13}C^\alpha$ nuclei in $^2H,^{13}C,^{15}N$-labeled molecules. The methods are applied to the third IgG-binding domain of protein G (GB3) and α-synuclein (αS) in complex with a detergent micelle. GB3 is a well-behaved protein which yields high-quality NMR spectra, and its atomic-resolution three-dimensional structure is known. It is therefore used as a model system to investigate the presence of any significant systematic errors and the accuracy of $^1D_{C'C^\alpha}$ measurements using the quantitative $J_{C'C^\alpha}$ methods. The αS/micelle complex study represents an application of the quantitative $J_{C'C^\alpha}$ methods to a larger, slower tumbling system.

Materials and methods

The two proteins used in the experiments are: $^{13}C,^{15}N$-labeled third IgG-binding domain of protein G (GB3, 56 residues, 6.5 kDa), and $^2H,^{13}C,^{15}N$-labeled α-synuclein (αS, 140 residues, 14.5 kDa) in complex with a sodium dodecyl sulfate (SDS) micelle with an effective rotational correlation time $\tau_c \approx 15$ ns at 25 °C, established on the basis of its ^{15}N relaxation properties. GB3 was overexpressed in *Escherichia coli* HMS174(DE3), using uniformly ^{13}C-enriched glucose and $^{15}NH_4Cl$ in M9 minimal medium (Ulmer et al., 2003). For the expression of αS, a single colony of freshly transformed *Escherichia coli* BL21(DE3) cells was used to inoculate 2 ml of LB medium and grown for 8 h at 37 °C. 25 ml of M9 medium, containing 1 g/l $^{15}NH_4Cl$ and 4 g/l glucose, was inoculated by 250 µl of the LB culture and grown overnight. 1.5 ml of this M9 culture were transferred to 25 ml of a fresh M9 medium prepared in D_2O, containing 1 g/l $^{15}NH_4Cl$ and 2 g/l ^{13}C-glucose, and grown for
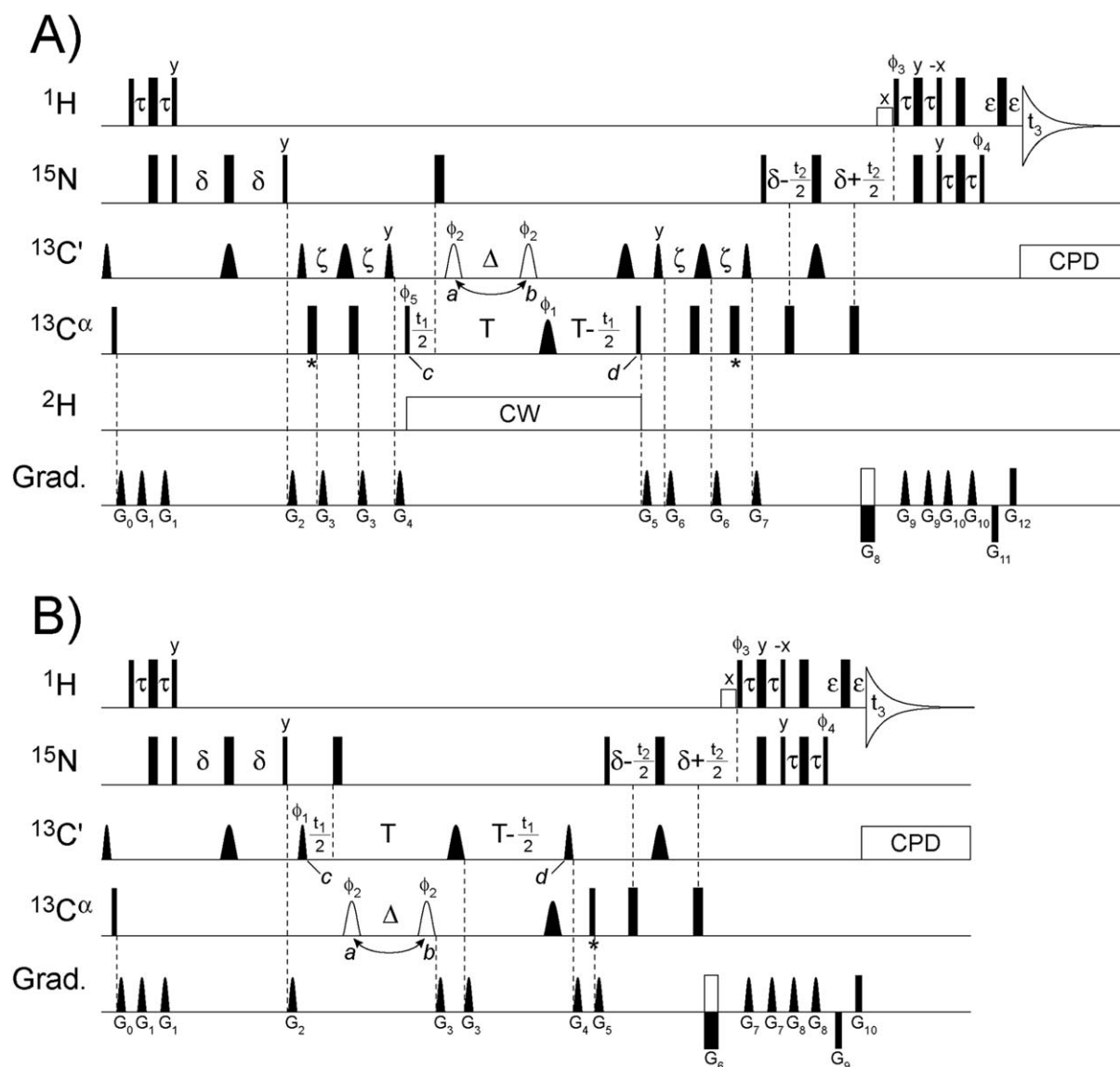
24 h. This culture was spun down and resuspended in 1 L of the final expression culture composed of ^{13}C,^{15}N-enriched M9 medium in D_2O, supplemented by 1 g/l of ^{2}H,^{13}C,^{15}N-labeled rich-medium supplement (Isogro, Isotec Inc., http://www.isotec.com). Protein expression was induced at $OD_{600} = 0.8$ for 4 h.

GB3 was oriented using 10 mg/ml filamentous phage Pf1 (Hansen et al., 1998) purchased from Asla Biotech Ltd. (Riga, Latvia, http://www.asla-biotech.com/asla-phage.htm), and αS was oriented in a 4.6% (w/v) negatively charged polyacrylamide gel (Meier et al., 2002; Ulmer et al., 2003), radially compressed from an initial diameter of 5.4 mm to 4.24 mm, i.e., axially stretched by a factor of ∼1.6 (Chou et al., 2001). Sample conditions: GB3, 1.5 mM, 40 mM sodium phosphate, pH 6.5, 0.08% (w/v) NaN_3, 93% H_2O, 7% D_2O, total sample volume 280 μl; αS, 0.5 mM, 75 mM SDS, 20 mM sodium phosphate, pH 7.4, 0.02% (w/v) NaN_3, 93% H_2O, 7% D_2O, total sample volume 280 μl. GB3 and αS data were collected at 25 °C, on Bruker DMX 500 and DRX 600 MHz spectrometers, respectively, using cryogenic, triple-resonance probeheads equipped with z-axis pulsed field gradients and optimized for ^{1}H-detection. Typical acquisition parameters used for the αS data sets

Figure 1. Pulse schemes of the (A) 3D TROSY-HN(CO)CA-QJ and (B) 3D TROSY-HNCO-QJ experiments. Narrow and wide pulses correspond to 90° and 180° flip angles (except for the open low-power 90° ^{1}H pulse), respectively. All pulses have phase x, unless indicated otherwise. The ^{1}H, ^{15}N, ^{2}H, ^{13}C′, and ^{13}C$^\alpha$ carriers are positioned at 4.75 (water), 116, 4.75, 177, and 56 ppm, respectively. ^{1}H pulses are applied at a field strength of 25 kHz, with the exception of the 1.35 ms water selective 90° pulse. All ^{15}N pulses are applied at a field strength of 5.3 kHz. A 2.0 kHz GARP composite pulse decoupling (CPD) field is used for ^{13}C′ during the acquisition of the FID, and in (A) a 0.6 kHz ^{2}H decoupling field is applied in continuous wave (CW) mode during t_1. The ^{13}C$^\alpha$ rectangular pulses are applied at field strengths of $\Delta\Omega/\sqrt{15}$ (for 90°) and $\Delta\Omega/\sqrt{3}$ (for 180°), where $\Delta\Omega$ is the frequency difference between the centers of the ^{13}C′ and ^{13}C$^\alpha$ chemical shift regions. All 90° and 180° ^{13}C shaped pulses have the profile of the center lobe of a $\sin x/x$ function, and durations of 75 μs and 150 μs, respectively (at 151 MHz ^{13}C frequency). Scheme (A), 3D TROSY-HN(CO)CA-QJ: ^{13}C$^\alpha$ inversion pulses during the 2ζ periods are applied immediately following (first 2ζ period) or prior to (second 2ζ period) the ^{13}C′ pulses; the off-resonance effect (Bloch-Siegert) ^{13}C$^\alpha$ compensation pulses are denoted by asterisks. The 180° ϕ_1 ^{13}C$^\alpha$ pulse has the RE-BURP profile, duration of 400 μs (at 151 MHz ^{13}C frequency), and is centered at 45 ppm for the uniform inversion of the ^{13}C$^\alpha$ and ^{13}C$^\beta$ spins. Delay durations: τ = 2.35 ms, δ = 12.5 ms, ζ = 4.3 ms, ε = 0.35 ms, Δ = T′ = 14.0 ms ≈ 3/(4 $^1J_{C'C^\alpha}$) (for the target value of $^1J_{C'C^\alpha}$ = 53.5 Hz) and T = T′ + $t^N_{180°}$ + $t^{C'}_{180°}$ ≈ 1/(2$^1J_{C^\alpha C^\beta}$), where $t^N_{180°}$ and $t^{C'}_{180°}$ are the durations of the ^{15}N and ^{13}C′ 180° pulses, respectively. Phase cycling: ϕ_1 = x, y; ϕ_2 = 2(x), 2($-x$); ϕ_3 = y; ϕ_4 = x; ϕ_5 = x; receiver = x, $-x$. Reference and attenuated spectra are acquired in an interleaved manner. For the reference spectrum the open ^{13}C′ pulse is applied in position a; for the attenuated spectrum in position b. States-TPPI phase cycling of ϕ_5 is used to obtain quadrature detection in the ^{13}C$^\alpha$ (F_1) dimension. Quadrature in the ^{15}N (F_2) dimension is achieved using the gradient- and sensitivity-enhanced method (Kay et al., 1992; Pervushin et al., 1998; Weigelt, 1998) in which two data sets are recorded for each t_2 increment: one set with the pulse phases indicated above, and a second set with phases ϕ_3 = $-y$ and ϕ_4 = $-x$ and the polarity of gradient G_8 inverted. For increased resolution in the ^{15}N dimension a semi-constant-time period can also be used (Kontaxis et al., 2000). The pulsed field gradients, sine-bell shaped with exception of G_8, G_{11} and G_{12} which are rectangular, are applied along the z-axis and have the following durations and strengths: $G_{0,1,2,3,4,5,6,7,8,9,10,11,12}$ = (2, 2, 1, 2, 1, 1, 2, 1, 2.8, 2, 2, 0.180, 0.104 ms) and (3, 12, 18, 15, 12, 9, 15, 24, −30, 18, 21, −30, 30 G/cm). Scheme (B), 3D TROSY-HNCO-QJ: The 180° ^{13}C$^\alpha$ shaped pulses are of the hyperbolic secant type and have a squareness level, μ, of 6 and durations of 2 ms (at 151 MHz ^{13}C frequency). The 90° ^{13}C$^\alpha$ pulse after the 2T period (denoted by an asterisk) suppresses minor E.COSY-like distortions of the cross-peaks in the F_3 dimension arising from the small fraction of ^{13}C′ nuclei evolving under $^1J_{C'C^\alpha}$ during t_1, for which the coupled ^{13}C$^\alpha$ spin is not inverted by the hyperbolic secant pulses. Delay durations: τ = 2.35 ms, δ = 12.5 ms, ζ = 4.3 ms, ε = 0.35 ms, Δ = T′ = 14.0 ms ≈ 3/(4$^1J_{C'C^\alpha}$) (for the target value of $^1J_{C'C^\alpha}$ = 53.5 Hz) and T = T′ + $t^N_{180°}$ + $t^{C^\alpha}_{180°}$ + t_G, where $t^N_{180°}$, $t^{C^\alpha}_{180°}$ and t_G are the durations of the ^{15}N and ^{13}C$^\alpha$ 180° pulses and gradient G_3, respectively. Phase cycling: ϕ_1 = x, $-x$; ϕ_2 = 2(x), 2($-x$); ϕ_3 = y; ϕ_4 = x; receiver = x, $-x$. Reference and attenuated spectra are acquired in an interleaved manner. For the reference spectrum the open ^{13}C$^\alpha$ pulse is applied in position a; for the attenuated spectrum in position b. States-TPPI phase cycling of ϕ_1 is used to obtain quadrature detection in the ^{13}C′ (F_1) dimension. Quadrature in the ^{15}N (F_2) dimension is achieved using the gradient- and sensitivity-enhanced method described in (A) with the polarity of gradient G_6 inverted. The pulsed field gradients, sine-bell shaped with exception of G_6, G_9 and G_{10} which are rectangular, are applied along the z-axis and have the following durations and strengths: $G_{0,1,2,3,4,5,6,7,8,9,10}$ = (2, 2, 1, 0.5, 1, 1, 2.8, 2, 2, 0.180, 0.104 ms) and (3, 12, 18, 15, 24, 9, −30, 18, 21, −30, 30 G/cm).

are as follows: 3D TROSY-HN(CO)CA quantitative $J_{C'C^\alpha}$ (TROSY-HN(CO)CA-QJ), two spectra were recorded in an interleaved fashion using the pulse scheme of Figure 1A. Each spectrum was acquired as a 96* × 32* × 512* data matrix with acquisition times of 27.6 ms (t_1, ^{13}C$^\alpha$), 24.2 ms (t_2, ^{15}N), and 56.8 ms (t_3, ^{1}H), using 4 scans per FID, and a total measurement time of 56 h for the pair of interleaved spectra; 3D TROSY-HNCO quantitative $J_{C'C^\alpha}$ (TROSY-HNCO-QJ), two spectra were recorded in an interleaved fashion using the pulse scheme of Figure 1B. Each spectrum was acquired as a 34* × 32* × 512* data matrix with acquisition times of 27.2 ms (t_1, ^{13}C′), 24.2 ms (t_2, ^{15}N), and 56.8 ms (t_3, ^{1}H), using 8 scans per FID, and a total measurement time of 40 h for the pair of interleaved spectra; 3D ^{13}C$^\alpha$-coupled TROSY-HNCO, the spectrum was acquired as a 98* × 40* × 512* data matrix with acquisition times of 79.2 ms (t_1, ^{13}C′), 23.3 ms (t_2, ^{15}N), and 56.8 ms (t_3, ^{1}H), using 4 scans per FID, and a total measurement time of 36 h.

All data sets were processed and analyzed using NMRPipe (Delaglio et al., 1995). For the quantitative $J_{C'C^\alpha}$ experiments the cross-peak positions were determined from the high signal-to-noise reference spectrum. Subsequently the intensity in both reference and attenuated spectra at those exact positions was measured by employing the 3D Fourier interpolation feature in NMRPipe.

Description of pulse schemes

The 3D triple-resonance experiments for the measurement of $^1J_{C'C^\alpha}$ in isotopically labeled proteins (Figure 1) are of the constant-time variety and are based on the well-known HN(CO)CA and HNCO schemes, employing the TROSY principle (Pervushin et al., 1997) in the ^{15}N and ^{1}H^N dimensions. Therefore, in the following we highlight only the unique features of the present experiments. The magnetization transfer for the 3D TROSY-HN(CO)CA (Figure 1A) and 3D
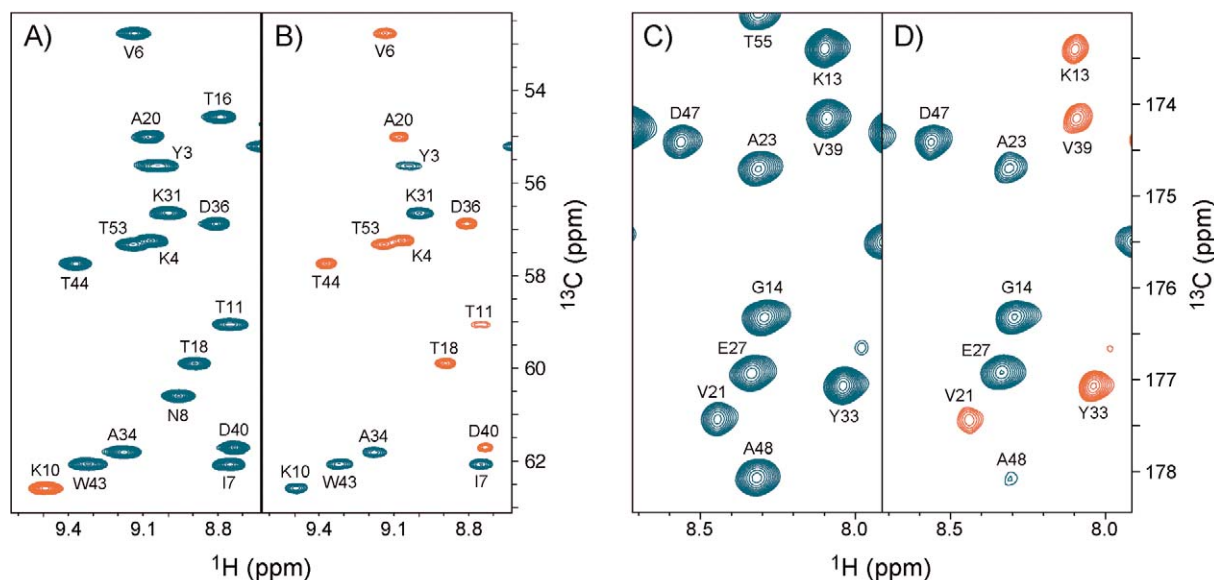
Figure 2. Small projected $^1\text{H}^\text{N}$-^{13}C regions (500 MHz) taken from (A) reference and (B) attenuated 3D HN(CO)CA-QJ spectra, and from (C) reference and (D) attenuated 3D HNCO-QJ spectra of ^{13}C,^{15}N-labeled GB3, in the presence of 10 mg/ml Pf1. Spectra were recorded using the regular Rance-Kay (Kay et al., 1992) versions of the 3D TROSY-HN(CO)CA-QJ and TROSY-HNCO-QJ schemes of Figure 1 (Supporting Information Figures S1 and S2). The residue numbers correspond to the $^1\text{H}^\text{N}$ frequency, and blue and red contours denote positive and negative cross-peaks, respectively. In (A) the K10 cross-peak, which corresponds to the $^{13}\text{C}^\alpha$ frequency of G9, is folded in the $^{13}\text{C}^\alpha$ dimension and has an opposite sign relative to the other cross-peaks due to the constant-time ($2T \approx 1/(^1 J_{\text{C}^\alpha\text{C}\beta})$) nature of the $^{13}\text{C}^\alpha$ evolution period (Vuister and Bax, 1992). Opposite cross-peak signs in (A) and (B) indicate $^1 J_{\text{C}'\text{C}^\alpha} + ^1 D_{\text{C}'\text{C}^\alpha} < 3/(4\text{T}')$; same cross-peak signs indicate $^1 J_{\text{C}'\text{C}^\alpha} + ^1 D_{\text{C}'\text{C}^\alpha} > 3/(4(\text{T}')$; absence of N8 and T16 cross-peaks in (B) indicates $^1 J_{\text{C}'\text{C}^\alpha} + ^1 D_{\text{C}'\text{C}^\alpha}$ values close to the null-condition, $3/(4\text{T}') \approx 53.5$ Hz. The same argument applies to (C) and (D), although the attenuated spectrum is subject to small systematic errors in cross-peak intensity due to the presence of 2–6% of $^{13}\text{C}'$-$^{12}\text{C}^\alpha$ spin pairs. As discussed in the text this does not significantly influence the accurate measurement of $^1 D_{\text{C}'\text{C}^\alpha}$.

TROSY-HNCO (Figure 1B) quantitative $J_{\text{C}'\text{C}^\alpha}$ experiments is given by pathways 1a and 1b, respectively:

$$^1\text{H}^\text{N} \overset{^1 J_{\text{NH}}}{\rightarrow} {}^{15}\text{N} \overset{^1 J_{\text{NC}'}}{\rightarrow} {}^{13}\text{C}' \overset{^1 J_{\text{C}'\text{C}^\alpha}}{\rightarrow} {}^{13}\text{C}^\alpha(t_1)$$
$$\overset{^1 J_{\text{C}'\text{C}^\alpha}}{\rightarrow} {}^{13}\text{C}' \overset{^1 J_{\text{NC}'}}{\rightarrow} {}^{15}\text{N}(t_2) \overset{^1 J_{\text{NH}}}{\rightarrow} {}^1\text{H}^\text{N}(t_3), \tag{1a}$$

$$^1\text{H}^\text{N} \overset{^1 J_{\text{NH}}}{\rightarrow} {}^{15}\text{N} \overset{^1 J_{\text{NC}'}}{\rightarrow} {}^{13}\text{C}'(t_1) \overset{^1 J_{\text{NC}'}}{\rightarrow} {}^{15}\text{N}(t_2)$$
$$\overset{^1 J_{\text{NH}}}{\rightarrow} {}^1\text{H}^\text{N}(t_3), \tag{1b}$$
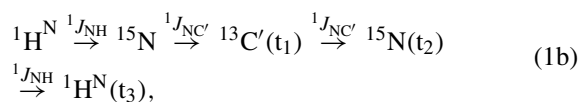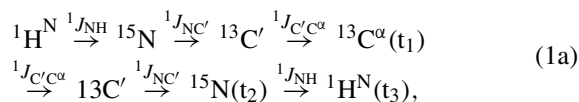
In both experiments $^1 J_{\text{C}'\text{C}^\alpha}$ is extracted from the ratio of cross-peak intensities in two interleaved 3D spectra recorded with different $^1 J_{\text{C}'\text{C}^\alpha}$ dephasing intervals. Although the cross-peak intensities are determined primarily by the magnitude of $^1 J_{\text{C}'\text{C}^\alpha}$, the effects of passive ^{13}C-^{13}C couplings, nonideal pulses and incomplete isotopic ^{13}C enrichment, which lead to systematic errors in the measured $^1 J_{\text{C}'\text{C}^\alpha}$ value, can also play a role. However, as discussed in the **Analysis of Errors** section, most of these effects can be neglected for the pulse schemes described here; consequently the simple model described below can be

used to provide reliable measurements of one-bond $^{13}\text{C}'$-$^{13}\text{C}^\alpha$ dipolar couplings. In particular we note that the 3D TROSY-HNCO-QJ pulse scheme of Figure 1B is not compensated for the effects of incomplete ^{13}C labeling. Although this can lead to substantial systematic errors in the $^1 J_{\text{C}'\text{C}^\alpha}$ values extracted from spectra recorded in isotropic and aligned phases when using the simple model described below (e.g., errors of up to ~0.4 Hz are obtained for 98% ^{13}C labeling efficiency and $^1 J_{\text{C}'\text{C}^\alpha}$ in the 48–60 Hz range), for weakly aligned proteins in the limit of nearly complete (i.e., >95%) ^{13}C labeling the systematic errors in $^1 J_{\text{C}'\text{C}^\alpha}$ (isotropic) and $^1 J_{\text{C}'\text{C}^\alpha} + ^1 D_{\text{C}'\text{C}^\alpha}$ (aligned) measurements almost completely cancel each other, yielding an accurate measurement of $^1 D_{\text{C}'\text{C}^\alpha}$. Alternatively, modified 3D TROSY-HNCO-QJ pulse schemes can be used (Supporting Information Figure S3), which are compensated for incomplete ^{13}C enrichment, albeit with a concomitant decrease in sensitivity.

In the following we describe a simple model for the extraction of $^1 J_{\text{C}'\text{C}^\alpha}$ from the ratio of cross-peak in-

tensities in two interleaved spectra recorded with different $^1J_{C'C^\alpha}$ dephasing intervals. The density matrix describing the magnetization at the beginning of the constant-time (2T) period in the TROSY-HN(CO)CA-QJ and TROSY-HNCO-QJ experiments (time point c in the pulse schemes) is given by Equations 2a and 2b, respectively:

$$\sigma_c = C_y^\alpha C_z' N_z(\Theta_1 \mathbf{1} + \Theta_2 H_z), \qquad (2a)$$

$$\sigma_c = C_y' N_z(\Phi_1 \mathbf{1} + \Phi_2 H_z), \qquad (2b)$$

where H, N, C', and C^α are the $^1H^N$, ^{15}N, $^{13}C'$, and $^{13}C^\alpha$ spin operators, respectively, and Θ_i and Φ_i ($i = 1,2$) are constants which depend on the magnetization transfer delays τ, δ and ζ. During the 2T periods (between time points c and d) the $^{13}C^\alpha$ (for the HN(CO)CA-QJ experiment) or $^{13}C'$ (for the HNCO-QJ experiment) antiphase coherence is allowed to evolve under $^1J_{C'C^\alpha}$ for time for $2(T' - \Delta) = 0$ for the reference spectrum (i.e., $^{13}C'$-$^{13}C^\alpha$ couplings are fully refocused) or $2T' = 28.0$ ms (i.e., $3/(2^1J_{C'C^\alpha})$ for the target value of $^1J_{C'C^\alpha} = 53.5$ Hz) for the attenuated spectrum, resulting in cross-peak intensities proportional to:

$$I_{ref} = A\cos[2\pi\,^1J_{C'C^\alpha}(T' - \Delta)] = A, \qquad (3a)$$

$$I_{att} = A\cos(2\pi\,^1J_{C'C^\alpha}T'), \qquad (3b)$$

where A is the reference cross-peak intensity, which depends on the exact sample conditions and the details of the experimental setup, and $\Delta = T' = 14.0$ ms (Figure 1 caption). Simple inspection of the resulting spectra provides information on the magnitude of $^1J_{C'C^\alpha}$ relative to the target value of 53.5 Hz: opposite cross-peak signs in the reference and attenuated spectra indicate $^1J_{C'C^\alpha} < 53.5$ Hz, same cross-peak signs indicate $^1J_{C'C^\alpha} > 53.5$ Hz, and absence of cross-peaks in the attenuated spectrum indicates $^1J_{C'C^\alpha}$ values close to the null-condition, $J = 3/(4T') = 53.5$ Hz. The precise value of $^1J_{C'C^\alpha}$ is obtained by fitting the experimental intensity ratio, I_{att}/I_{ref}, to the function:

$$\frac{I_{att}}{I_{ref}} = \cos(2\pi\,^1J_{C'C^\alpha}T'). \qquad (4)$$

Note that for optimal resolution and sensitivity the 2T period is used to simultaneously encode the $^{13}C^\alpha$ or $^{13}C'$ frequency in t_1. Furthermore, for the HN(CO)CA-QJ experiment this period corresponds to the condition $2T \approx 1/^1J_{C^\alpha C^\beta}$), which scales the cross-peak intensities by an additional factor of $\cos(2\pi\,^1J_{C^\alpha C^\beta}T) \approx -1$ (except for glycine residues)

and results in nearly ideal refocusing of the one-bond $^{13}C^\alpha$-$^{13}C^\beta$ couplings (Vuister and Bax, 1992). The quantitative $J_{C'C^\alpha}$ experiments described in this work provide precise measurements of $^1J_{C'C^\alpha}$ for proteins that yield high S/N ($\sim$30:1 or higher) 3D HNCO and HN(CO)CA spectra. The selection of one method over another will depend on the relative $^{13}C'$ and $^{13}C^\alpha$ transverse relaxation rates for the protein under consideration at the magnetic field strength employed and the spectral resolution; due to the relatively long $^{13}C^\alpha$ T_2 in deuterated samples the TROSY-HN(CO)CA-QJ experiment is most applicable to high molecular weight $^2H,^{13}C,^{15}N$-labeled proteins studied at high magnetic fields. Although the HN(CO)CA-QJ experiment can also be used to measure $^1J_{C'C^\alpha}$ in small $^{13}C,^{15}N$-labeled protonated proteins as demonstrated for GB3, it generally will not be very useful in larger systems of this type. For $^{13}C,^{15}N$-labeled proteins a TROSY or a regular gradient- and sensitivity-enhanced (Rance–Kay type) (Kay et al., 1992) HNCO-QJ experiment (Supporting Information Figure S2) is most applicable. Finally we note that the quantitative $J_{C'C^\alpha}$ experiments presented here can be easily implemented as the corresponding 2D versions with frequency labeling in t_1 or t_2. However, since the experiments are of the constant-time variety, at most a small gain in sensitivity per unit time is obtained by setting a particular evolution period to zero and performing the experiments in 2D fashion.

Experimental results

Application to protein G

In Figure 2 we show small regions of the reference and attenuated spectra recorded for $^{13}C,^{15}N$-labeled GB3, aligned in 10 mg/ml Pf1, using the Rance-Kay versions of the 3D TROSY-HN(CO)CA-QJ (A, B) and 3D TROSY-HNCO-QJ (C, D) experiments (Supporting Information Figures S1 and S2). All 55 cross-peaks are resolved in the 3D spectra and permit the measurement of the corresponding $^1D_{C'C^\alpha}$ couplings (Supporting Information Table S1). The $^1D_{C'C^\alpha}$ values obtained from the quantitative $J_{C'C^\alpha}$ methods are in excellent agreement, with a pairwise rms difference of 0.08 Hz; this is consistent with uncertainties of ca. 0.05 Hz for the individual $^1D_{C'C^\alpha}$ measurements, estimated on the basis of the average S/N ratio of $\sim$400:1 for GB3 (see Analysis of errors section) and observed experimentally in duplicate 3D HN(CO)CA-QJ spectra. Figure 3 compares the $^1D_{C'C^\alpha}$ couplings
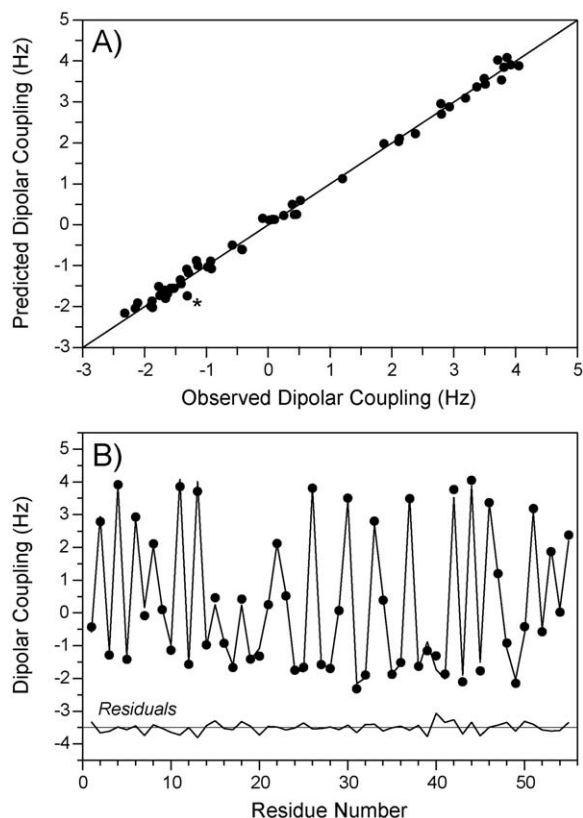
Figure 3. (A) Correlation between $^1D_{C'C^\alpha}$ values measured using the HN(CO)CA-QJ method, and values predicted for GB3 using an alignment tensor obtained from the best-fit of the $^1D_{C'C^\alpha}$ values to a GB3 structure. The GB3 reference structure used was previously obtained by refining the 1.1 Å X-ray structure (Derrick and Wigley, 1994) using a nearly complete set of backbone $^1H^N$-^{15}N, $^{13}C^\alpha$-$^1H^\alpha$, $^{13}C'$-$^{13}C^\alpha$, $^{13}C'$-^{15}N dipolar couplings and 34 experimentally validated hydrogen bond restraints (structure denoted as refined-II in Ulmer et al. (Ulmer et al., 2003)). The correlation coefficient, R_P, equals 0.998, and the rmsd between measured and predicted dipolar couplings is 0.14 Hz. Alignment tensor parameters: D_a^{NH} = 10.3 Hz, R = 0.05. The asterisk denotes residue D40 (see text). (B) Overlay of measured (●) and predicted (—) $^1D_{C'C^\alpha}$ values for GB3 as a function of residue number.

extracted from the HN(CO)CA-QJ experiment and the best-fit values calculated by using the SVD method (Losonczi et al., 1999) for a GB3 structure obtained by refining the 1.1 Å X-ray structure (Derrick and Wigley, 1994) (PDB entry 1IGD) using a nearly complete set of backbone $^1H^N$-^{15}N, $^{13}C^\alpha$-$^1H^\alpha$, $^{13}C'$-$^{13}C^\alpha$, $^{13}C'$-^{15}N dipolar couplings and 34 experimentally validated hydrogen bond restraints (structure denoted as refined-II in Ulmer et al. (2003); closely related PDB entries 1P7E and 1P7F result in essentially identical fits). The correlation coefficient, R_P, is 0.998, and the rms difference between the observed and predicted couplings

is 0.14 Hz. Remarkably, the measured dipolar couplings are in even better agreement with the refined structure than the input $^{13}C'$-$^{13}C^\alpha$ couplings used for the refinement. The correlation between observed and calculated $^1D_{C'C^\alpha}$ couplings as a function of residue number (Figure 3B) reveals no consistent outliers for any particular region of the structure, although the largest deviation, ca. 0.4 Hz, is observed for the turn residue D40 (indicated by an asterisk in Figure 3A), which is subject to increased internal dynamics based on ^{15}N relaxation data (Hall and Fushman, 2003) and none of its dipolar couplings were used as restraints in the original refinement (Ulmer et al., 2003). A best-fit of the measured $^1D_{C'C^\alpha}$ couplings to the 1.1 Å X-ray structure (1IGD) (backbone coordinate rmsd of 0.32 Å relative to the refined NMR structure) was also calculated, with R_P = 0.994, rmsd = 0.23 Hz, and Q = 0.123 (where Q = rms(D_{pred} − D_{obs})/[D_a^2 $(4 + 3R^2)/5]^{1/2}$ is the quality factor, with D_a and R denoting the magnitude and rhombicity of the alignment tensor, respectively (Bax et al., 2001)). For comparison with the quantitative $J_{C'C^\alpha}$ methods, $^1D_{C'C^\alpha}$ couplings were measured from the frequency difference in $^{13}C'$-{$^{13}C^\alpha$} doublet components in conventional $^{13}C^\alpha$-coupled 3D HNCO spectra (Supporting Information Table S1). The values obtained using the $^{13}C^\alpha$-coupled 3D HNCO and the 3D HN(CO)CA-QJ and HNCO-QJ methods are in very good agreement (rms difference of 0.14 Hz relative to each set of quantitative $J_{C'C^\alpha}$ measurements), and best-fits to the GB3 structure for $^1D_{C'C^\alpha}$ from the $^{13}C^\alpha$-coupled 3D HNCO data sets resulted in R_P = 0.997 and rmsd = 0.16 Hz for the NMR-refined GB3 structure, and R_P = 0.993, rmsd = 0.25 Hz, and Q = 0.131 for 1IGD.

Application to α-synuclein

αS is a 140-residue protein whose misfolding is believed to play an important role in the pathogenesis of Parkinson's disease. Previous NMR studies show that the protein, which is natively unstructured in solution, binds to vesicles and detergent micelles with its N-terminal region in a predominately α-helical conformation, while the C-terminal region remains unfolded and does not associate with lipids (Eliezer et al., 2001; Chandra et al., 2003). Our studies of αS bound to an SDS micelle indicate an effective rotational correlation time (τ_c) of ca. 15 ns at 25 °C for the protein, and in agreement with the published data, we find that the majority of the first 95 N-terminal residues (amino acids 2-96) adopt an α-helical fold and interact
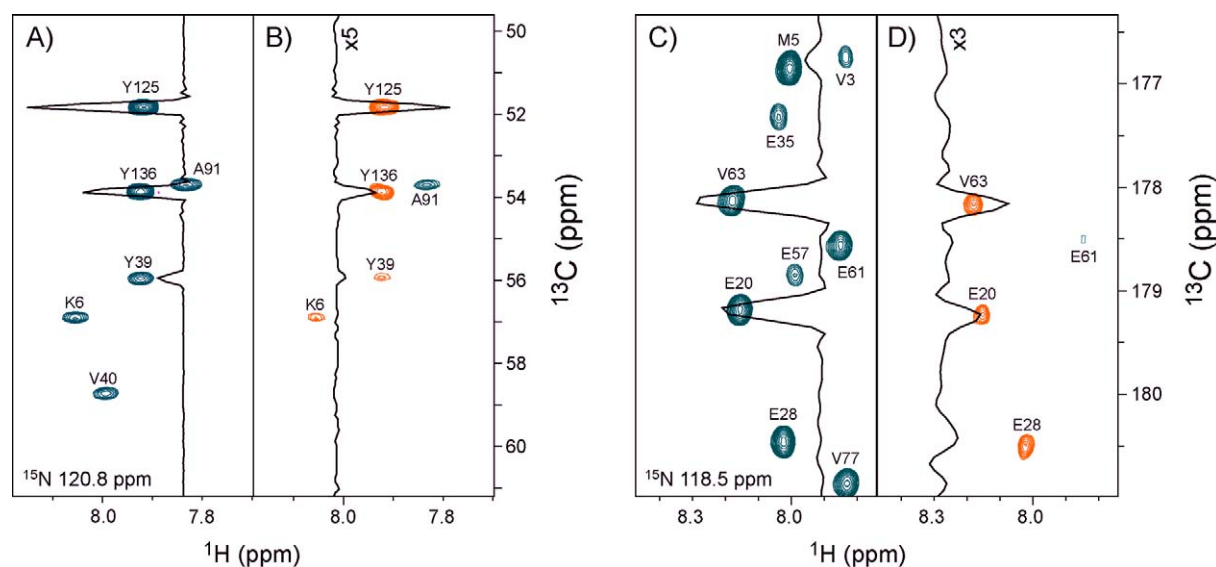
Figure 4. Small $^1H^N-^{13}C$ regions (600 MHz) taken from (A) reference and (B) attenuated 3D TROSY-HN(CO)CA-QJ spectra and from (C) reference and (D) attenuated 3D TROSY-HNCO-QJ spectra of $^2H,^{13}C,^{15}N$-labeled αS in complex with an SDS micelle and aligned in a stretched polyacrylamide gel. Positive (blue) and negative (red) cross-peaks are drawn with the lowest contour level at 25, 5, 15 and 5 times the rms noise level for (A), (B), (C) and (D), respectively. Inset in the spectra are 1D traces taken at a ^1H frequency of 7.92 ppm (A, B), and at a ^1H frequency of 8.18 ppm (C, D). Note that the 1D traces in (B) and (D) have been multiplied by a factor of 5 and 3, respectively, relative to the corresponding traces in (A) and (C).

with the micelle surface, while the C-terminal tail is unstructured in solution.

In Figure 4 we show small regions of reference and attenuated spectra recorded for the $^2H,^{13}C,^{15}N$-labeled αS/micelle complex aligned in a stretched polyacrylamide gel using the 3D TROSY-HN(CO)CA-QJ (A, B) and 3D TROSY-HNCO-QJ (C, D) methods. The resolution and cross-peak intensity observed in the spectra demonstrate that by employing a cryogenic probehead high-quality $^1D_{C'C^\alpha}$ measurements can be performed for a sample of 0.5 mM protein with a relatively long τ_c. For the aligned sample the average S/N ratio for the structured residues (2–96) is ~90:1 in the reference spectra acquired for both types of quantitative $J_{C'C^\alpha}$ experiments, and for the residues in the unstructured C-terminal tail the average S/N ratio is approximately five-fold higher, as indicated by the $^1H^N$ Y125 and Y136 correlations in the 1D trace in Figure 4A; for the isotropic sample the average S/N ratio for residues 2–96 is ~200:1 (data not shown). The measurements in αS (Supporting Information Table S2) are compared with one another in Figure 5. Since no high resolution structure is currently available for the micelle bound protein, the $^1D_{C'C^\alpha}$ values obtained from F_1 doublets of a conventional $^{13}C^\alpha$-coupled 3D TROSY-HNCO

spectrum are plotted against the corresponding values extracted from 3D TROSY-HNCO-QJ and TROSY-HN(CO)CA-QJ experiments. The $^{13}C^\alpha$-coupled 3D TROSY-HNCO spectrum permitted the measurement of 123 out of 134 possible dipolar couplings (the couplings for the C-terminal residue and the residues preceding the five prolines are not accessible in HNCO- and HN(CO)CA-based methods), with partial overlap between the $^{13}C^\alpha = |\alpha\rangle$ and $^{13}C^\alpha = |\beta\rangle$ doublet components observed for 12 residues in the spectra recorded in the isotropic and/or aligned phase (Supporting Information Table S2); 126 and 125 dipolar couplings could be obtained from the 3D TROSY-HN(CO)CA-QJ and 3D TROSY-HNCO-QJ spectra, respectively. The $^1D_{C'C^\alpha}$ values determined using the different methods are in good agreement with correlation coefficients between ca. 0.96 and 0.99, and we note that the agreement between any two quantitative $J_{C'C^\alpha}$ experiments is generally substantially better than the agreement between $^1D_{C'C^\alpha}$ determined using either of the quantitative $J_{C'C^\alpha}$ methods and those measured from the frequency difference of doublet components in the $^{13}C^\alpha$-coupled 3D TROSY-HNCO spectrum (Figure 5 and Supporting Information Figure S4). The largest deviation (ca. 0.8 Hz) between the quantitative $J_{C'C^\alpha}$ methods is observed for residue T92

Table 1. Estimation of $^{13}C^\alpha$ enrichment according to residue type for $^2H, ^{13}C, ^{15}N$-labeled αS

Residue type	Number of residues[a]	δJ (Hz)[b]	$^{13}C^\alpha$ enrichment (%)[c]
Ala	17	0.30 ± 0.08	97.4 ± 0.7
Asp	5	0.28 ± 0.04	97.5 ± 0.4
Glu	17	0.42 ± 0.08	96.3 ± 0.7
Phe	2	0.56 ± 0.04	95.1 ± 0.3
Gly	18	0.05 ± 0.19	99.6 ± 1.7
His	1	0.42	96.3
Ile	2	0.67 ± 0.06	94.1 ± 0.5
Lys	15	0.53 ± 0.12	95.3 ± 1.1
Leu	3	0.37 ± 0.09	96.7 ± 0.8
Met	1	0.50	95.6
Asn	3	0.18 ± 0.07	98.4 ± 0.6
Pro	5	0.68 ± 0.02	94.0 ± 0.2
Gln	6	0.41 ± 0.07	96.4 ± 0.6
Ser	4	0.56 ± 0.12	95.1 ± 1.1
Thr	7	0.80 ± 0.11	93.0 ± 1.0
Val	17	0.75 ± 0.14	93.4 ± 1.2
Tyr	4	0.45 ± 0.07	96.0 ± 0.6
All residues	127	0.44 ± 0.25	96.1 ± 2.2

The $^{13}C^\alpha$ labeling efficiency was obtained by comparing the apparent $^1J_{C'C^\alpha}$ values in isotropic αS measured using the 3D TROSY-HN(CO)CA-QJ and 3D TROSY-HNCO-QJ methods.
[a]Only residues for which $^1J_{C'C^\alpha}$ could be determined using both quantitative $J_{C'C^\alpha}$ methods are included in the analysis.
[b]$\delta J = {}^1J_{C'C^\alpha}$ (HNCO-QJ) $- {}^1J_{C'C^\alpha}$ (HN(CO)CA-QJ), is the difference between the $^1J_{C'C^\alpha}$ values for αS in the isotropic phase calculated using Equation 4 from 3D TROSY-HNCO-QJ (Figure 1B) and 3D TROSY-HN(CO)CA-QJ (Figure 1A) spectra. Note that $\delta J > 0$, because $^1J_{C'C^\alpha}$ (HNCO-QJ) $> {}^1J_{C'C^\alpha}$ (HN(CO)CA-QJ) due to the effects of incomplete $^{13}C^\alpha$ enrichment on the HNCO-QJ experiment.
[c]The $^{13}C^\alpha$ labeling efficiency, λ, is given by $\lambda(\%) = 100 \times \{1 - \cos[\pi(1/2 - 2T'\delta J)]\}$, which is obtained from Equations 4 and 7 for J equal to the target value, $^1J_{C'C^\alpha} = 3/(4T') = 53.5$ Hz (i.e., T' = 14.0 ms). Note that the HN(CO)CA-QJ experiment indicates the average value of 52.8 Hz ± 0.4 Hz for $^1J_{C'C^\alpha}$ in αS, which is sufficiently close to the target value of 53.5 Hz.

(indicated by an asterisk in Figure 5C). We note that this discrepancy is in large part due to the fact that Thr residues are among the most poorly ^{13}C labeled amino acids in αS, with an estimated labeling efficiency of ∼93% (Table 1), combined with a large and negative value of $^1D_{C'C^\alpha}$ for T92, and the use of the single-parameter model (Equation 4) to extract the value of $^1J_{C'C^\alpha}$ from the 3D TROSY-HNCO-QJ spectra (see Analysis of errors section). When incomplete $^{13}C^\alpha$ labeling is taken into account during the analysis of the TROSY-HNCO-QJ spectra, the discrepancy in the $^1D_{C'C^\alpha}$ measurements for T92 is reduced by ∼40% to 0.5 Hz. Furthermore, we note that $^1D_{C'C^\alpha}$ values determined for T92 using the 3D TROSY-HN(CO)CA-QJ method and a modified 3D TROSY-HNCO-QJ experiment (Supporting Information Figure S3), both of which are compensated for the effects of incomplete ^{13}C labeling, agree to within 0.1 Hz (Supporting Information Table S2 and Figure S4).

The structured α-helical region of the protein displays lower S/N ratios (residues 2–96), and consequently higher pairwise rmsd's of 0.44 Hz (Figure 5A, F_1 doublets vs. HN(CO)CA-QJ), 0.45 Hz (Figure 5B, F_1 doublets vs. HNCO-QJ) and 0.23 Hz (Figure 5C, HN(CO)CA-QJ vs. HNCO-QJ). Assuming that the errors between the different measurements are uncorrelated, these pairwise rmsd's can be used to estimate the following uncertainties $^1D_{C'C^\alpha}$ in measurements for the individual experiments: 0.15 Hz for HN(CO)CA-QJ, 0.18 Hz for HNCO-QJ, and 0.41 Hz

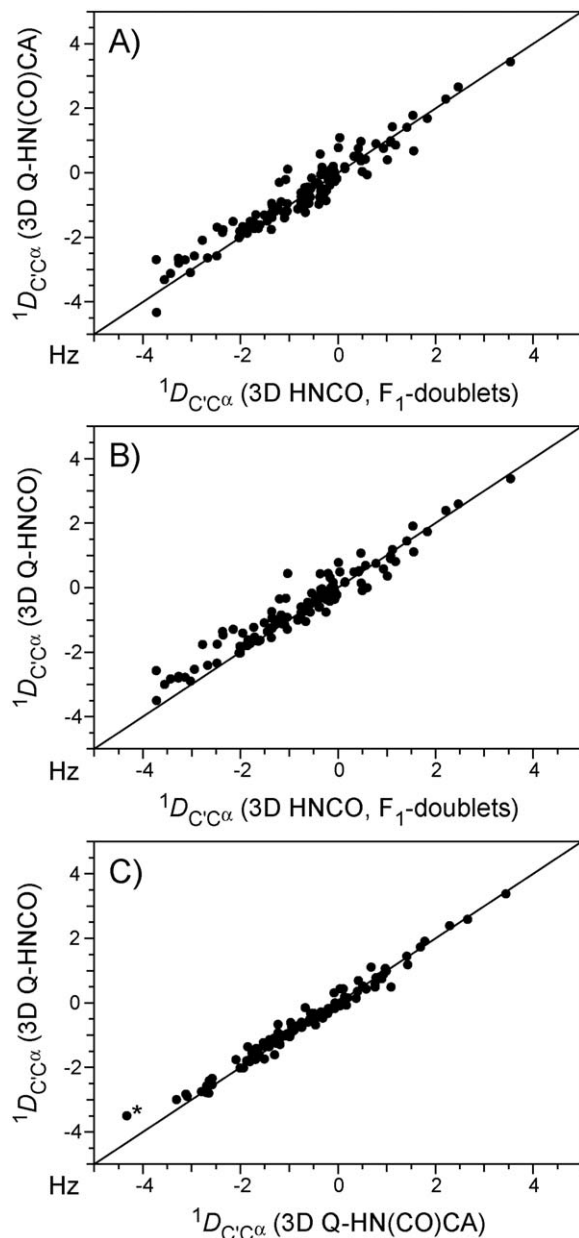*Figure 5.* Comparison of $^{1}D_{C'C^{\alpha}}$ values measured with three different methods in ^{2}H,^{13}C,^{15}N-labeled αS complexed with an SDS micelle, for the 118 $^{1}D_{C'C^{\alpha}}$ values that could be determined by all three methods. (A) $^{1}D_{C'C^{\alpha}}$ measured from F_{1} doublets of a conventional ^{13}C$^{\alpha}$-coupled 3D TROSY-HNCO spectrum versus $^{1}D_{C'C^{\alpha}}$ from a 3D TROSY-HN(CO)CA-QJ spectrum (pulse scheme of Figure 1A). (B) $^{1}D_{C'C^{\alpha}}$ measured from F_{1} doublets of a ^{13}C$^{\alpha}$-coupled 3D TROSY-HNCO spectrum versus $^{1}D_{C'C^{\alpha}}$ from a 3D TROSY-HNCO-QJ spectrum (pulse scheme of Figure 1B). (C) $^{1}D_{C'C^{\alpha}}$ measured from a 3D TROSY-HN(CO)CA-QJ spectrum versus $^{1}D_{C'C^{\alpha}}$ from a 3D TROSY-HNCO-QJ spectrum. The asterisk indicates the measurement for residue T92 (see text). The pairwise rms deviations for residues 2-96 are 0.44 Hz for (A), 0.45 Hz for (B) and 0.23 Hz for (C); for all residues the rms deviations are 0.38 Hz for (A), 0.39 Hz for (B) and 0.20 Hz for (C).

for ^{13}C$^{\alpha}$-coupled HNCO F_{1} doublets. These uncertainties represent a nearly two-fold improvement in precision for the quantitative J$_{C'C^{\alpha}}$ methods relative to the conventional ^{13}C$^{\alpha}$-coupled HNCO measurements, and agree reasonably well with values estimated independently based on the S/N ratios observed in the different spectra (see Analysis of errors section). For the ^{13}C$^{\alpha}$-coupled 3D TROSY-HNCO, 3D TROSY-HNCO-QJ, and 3D TROSY-HN(CO)CA-QJ the average S/N ratio for residues 2–96 in isotropic (aligned) phase was ca. 100:1 (60:1), 220:1 (95:1), 200:1 (90:1), respectively, and the average uncertainties in $^{1}D_{C'C^{\alpha}}$ were 0.29 Hz, 0.15 Hz, and 0.16 Hz, respectively (for the ^{13}C$^{\alpha}$-coupled HNCO we used the relation $\Delta D = LW/SN$ to approximate the lower limit for the uncertainty in the dipolar coupling (Kontaxis et al., 2000; Bax et al., 2001), where LW is the linewidth at half-height and SN is the signal-to-noise ratio for the aligned phase).

Analysis of errors

In the following section we consider the effects of random noise, passive ^{13}C-^{13}C couplings, incomplete isotopic ^{13}C enrichment and nonideal pulses on the measurement of $^{1}J_{C'C^{\alpha}}$ when using the quantitative J$_{C'C^{\alpha}}$ methods. Although in principle Equation 4 can be modified to account for the systematic errors due to these effects, we demonstrate below that for a reliable measurement of $^{1}D_{C'C^{\alpha}}$ in weakly aligned proteins such errors can typically be neglected (some exceptions may occur for relatively low levels of ^{13}C enrichment, as noted above for αS residue T92 and discussed in more detail below).

Effect of random noise

In analogy to other quantitative J correlation methods, the estimated random error in the J value extracted from HN(CO)CA-QJ and HNCO-QJ spectra using Equation 4 is dominated by the random noise in the attenuated spectrum and equals (Chou et al., 2000)

$$\Delta J = \frac{\sigma}{2\pi AT'}, \qquad (5)$$

where σ is the rms noise, A is the reference cross-peak intensity (i.e., S/N ratio in the reference spectrum is A/σ), and T' = 14.0 ms. For example, for a reference spectrum with a S/N ratio of 30:1, a random error of less than 0.4 Hz is obtained in the extracted value of J. Although the effect of the random noise increases

when the condition $4JT'/3 = 1$ is not satisfied, Equation 5 provides a reasonable approximation provided that the coupling is within ~5 Hz of the selected target value of $3/(4T') \approx 53.5$ Hz; this will typically be the case for weakly aligned proteins.

Effect of passive couplings

For both quantitative $J_{C'C^\alpha}$ experiments the one-bond (active) coupling of interest, $^1J_{C'C^\alpha}$, and all other (passive) couplings between the $^{13}C'$ ($^{13}C^\alpha$) nucleus and $^{13}C^\alpha$ ($^{13}C'$) spins are refocused in the reference experiment. However, all couplings contribute to the dephasing of the transverse ^{13}C coherences (Equation 2) in the attenuated spectra, resulting in:

$$\frac{I_{att}}{I_{ref}} = \cos(2\pi\,^1J_{C'C^\alpha}T')\Pi_i\cos(2\pi J_p^i T'), \qquad (6)$$

where J_p^i denotes the ith passive coupling. Figure 6 demonstrates the effect of the presence of a single passive $^{13}C'$-$^{13}C^\alpha$ coupling on the measurement of $^1J_{C'C^\alpha}$. A simple system of three ^{13}C spins (e.g., one $^{13}C'$ and two $^{13}C^\alpha$, or one $^{13}C^\alpha$ and two $^{13}C'$) is considered with the following couplings: $^1J_{C'C^\alpha}$ (the one-bond active $^{13}C'$-$^{13}C^\alpha$ coupling in the 48–60 Hz range) and J_p (a passive $^{13}C'$-$^{13}C^\alpha$ coupling of 2 or 4 Hz). For each coupling topology we use Equation 6 to calculate an I_{att}/I_{ref} ratio as a function of the one-bond active coupling, and subsequently fit this ratio using the single-coupling model of Equation 4 to extract an apparent $^1J_{C'C^\alpha}$. It is evident that the magnitude of the systematic error introduced by the passive coupling scales roughly with the square of the offset of the actual coupling from the target value (Chou et al., 2000) (for an active coupling equal to the target value, 53.5 Hz in this case, no error is introduced due to the presence of the passive coupling). Since the magnitude of the systematic error will typically be close to zero for the isotropic phase ($^1J_{C'C^\alpha}$ is within ~1 Hz of the target value) but can be larger for the aligned phase, any substantial error will propagate directly into the measurement of $^1D_{C'C^\alpha}$.

Fortunately, in ^{13}C enriched proteins the passive couplings are sufficiently small and can typically be neglected for both quantitative $J_{C'C^\alpha}$ pulse schemes presented here. For the HN(CO)CA-QJ scheme, for all residues except Asx and Glx we only need to consider $^2J_{C'C^\alpha}$, which is on average ca. 0.7 Hz in proteins (Hu and Bax, 1997), and $^2D_{C'C^\alpha}$, which has a magnitude of < 1 Hz based on calculations for the Pf1 aligned GB3 sample; thus if we assume a maximum $^2J_{C'C^\alpha}$ +
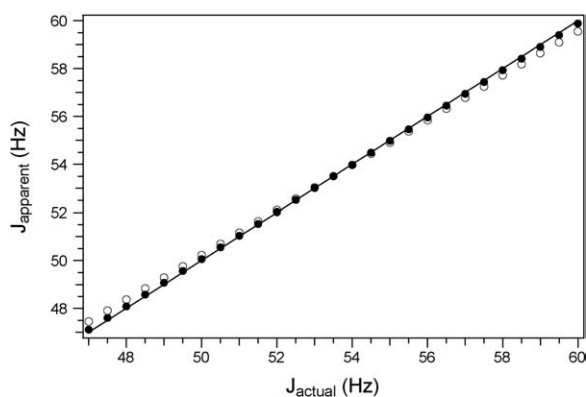

Figure 6. The effect of passive $^{13}C'$-$^{13}C^\alpha$ couplings on the measurement of $^1J_{C'C^\alpha}$. Ratios I_{att}/I_{ref} are calculated using Equation 6 as a function of the active (actual) J coupling for a passive $^{13}C'$-$^{13}C^\alpha$ coupling of 2 Hz ($\bullet$) or 4 Hz ($\circ$), and subsequently calculated using the single-coupling model of Equation 4 to extract an apparent $^1J_{C'C^\alpha}$. The solid line corresponds to $J_{apparent} = J_{actual}$.
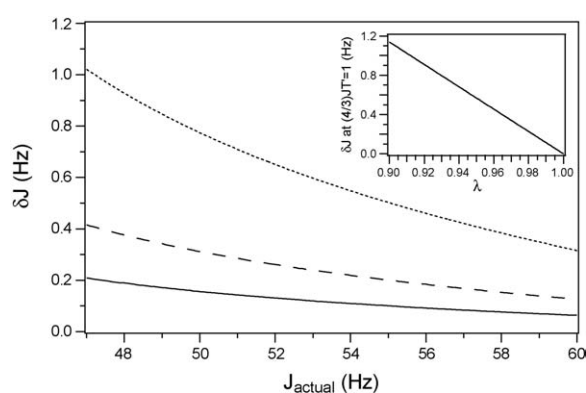

Figure 7. Effect of incomplete ^{13}C enrichment on measurement of $^1J_{C'C^\alpha}$ using the HNCO-QJ method of Figure 1B. Plots of the difference, δJ, between the apparent J coupling extracted using Equation 4 and the actual J coupling are shown for ^{13}C labeling efficiencies of 99% (solid line), 98% (dashed line) and 95% (dotted line). The inset in the figure shows a plot of δJ at the target J value as a function of ^{13}C labeling efficiency, λ, (cf., Table 1).

$^2D_{C'C^\alpha}$ coupling of 1.5 Hz for non-Asx/Glx residues the resulting error is at most ca. 0.05 Hz for a protein with $D_a^{NH} \approx 12.5$ Hz, which typically will be substantially smaller than the random error. For Asx residues, $^2J_{C^\alpha C^\gamma}$ is also expected to be at most 1 Hz with equally small dipolar contributions. Also including the 1.5 Hz backbone $^2J_{C'C^\alpha} + ^2D_{C'C^\alpha}$ couplings results in maximum errors of ca. 0.1 Hz. For Glx residues, $^3J_{C^\alpha C^\delta}$ depends on the χ_2 angle and could be as large as 4 Hz for a χ_2 angle of 180°, which would result in errors as large as 0.35 Hz.

For the HNCO-QJ scheme we mainly need to consider the backbone $^2J_{C'C^\alpha}$ and $^2D_{C'C^\alpha}$ couplings as

discussed above for the HN(CO)CA-QJ scheme, although $^2J_{C'C^\alpha}$ (ca. 1 Hz) and $^3J_{C'C^\beta}$ (< 3 Hz) (Hu and Bax, 1997) may contribute as well for C^β spins that are within the bandwidth of the C^α selective inversion pulses (e.g., Ser and Thr).

Effect of incomplete ^{13}C labeling

The HN(CO)CA-QJ pulse scheme (Figure 1A) is not affected by incomplete ^{13}C enrichment, since all observable magnetization has been transferred from $^{13}C'$ to $^{13}C^\alpha$ and back to $^{13}C'$ during the 2ζ periods bracketing the $^1J_{C'C^\alpha}$ dephasing period. Therefore, the following discussion is limited to the 3D TROSY-HNCO-QJ pulse scheme of Figure 1B, which is not compensated for the effects of incomplete ^{13}C enrichment. We note here that 3D TROSY-HNCO-QJ pulse schemes can be designed, which are compensated for incomplete ^{13}C labeling (Supporting Information Figure S3), albeit with a concomitant decrease in sensitivity.

For the HNCO-QJ pulse scheme, a small fraction of $^{13}C'$ atoms (typically <5% for a uniformly ^{13}C labeled protein) are bonded to $^{12}C^\alpha$ instead of $^{13}C^\alpha$ and are therefore not dephased during the 2T period. The resulting I_{att}/I_{ref} ratio (ignoring any long-range $^{13}C'$-$^{13}C^\alpha$ couplings) is then given by:

$$\frac{I_{att}}{I_{ref}} = \lambda \cos(2\pi \, {}^1J_{C'C^\alpha} T') + \varepsilon, \qquad (7)$$

where λ is the fraction of $^{13}C'$ spins coupled to $^{13}C^\alpha$ (ca. 0.95–0.99 for a fully ^{13}C labeled protein), and $\varepsilon = 1 - \lambda$ is the fraction of $^{13}C'$-$^{12}C^\alpha$ spin pairs. The small systematic change in the cross-peak intensity in the attenuated spectra can lead to substantial systematic errors in $^1J_{C'C^\alpha}$ values extracted using Equation 4 from data recorded in isotropic and aligned phases. Simulations shown in Figure 7 indicate errors of up to ca. 0.4 and 1 Hz, respectively, for 98% and 95% ^{13}C labeling efficiencies and $^1J_{C'C^\alpha}$ in the 48–60 Hz range. In addition, for each ^{13}C labeling efficiency the discrepancy between the actual $^1J_{C'C^\alpha}$ coupling and the apparent $^1J_{C'C^\alpha}$ coupling obtained using the simple model in Equation 4 is largest for large and negative $^1D_{C'C^\alpha}$ values. However, the simulations and experimental results in GB3 and αS indicate that for weakly aligned proteins in the limit of nearly complete (i.e., > 95%) ^{13}C labeling the systematic errors in $^1J_{C'C^\alpha}$ (isotropic) and $^1J_{C'C^\alpha} + {}^1D_{C'C^\alpha}$ (aligned) measurements will nearly cancel each other, yielding an accurate measurement of $^1D_{C'C^\alpha}$.

Finally, we note that we can use the fact that the 3D TROSY-HNCO-QJ pulse scheme of Figure 1B is not compensated for incomplete ^{13}C enrichment, to estimate the $^{13}C^\alpha$ labeling efficiency for the protein under study by comparing $^1J_{C'C^\alpha}$ values measured in the isotropic phase using the 3D TROSY-HNCO-QJ experiment and a method fully compensated for incomplete ^{13}C labeling (e.g., 3D TROSY-HN(CO)CA-QJ pulse scheme of Figure 1A). This analysis was performed for $^2H,^{13}C,^{15}N$-labeled αS and the results are summarized in Table 1. On average we estimate the $^{13}C^\alpha$ labeling efficiency in αS to be 96 ± 2%. Interestingly, the $^{13}C^\alpha$ labeling efficiencies display a pronounced dependence on the amino acid type, with Gly, Ala, Asp and Asn residues showing the highest (ca. 98–99%) labeling efficiencies, and Thr, Val and Pro residues being the most poorly labeled (ca. 93–94% labeling efficiency).

Effect of pulse imperfections

In the following we consider the potential systematic errors (of two distinct origins) on the extracted $^1J_{C'C^\alpha}$ values, introduced by nonideal inversion and refocusing ^{13}C pulses applied during the 2T dephasing periods. First, the imperfect inversion by the open $^{13}C'$ ($^{13}C^\alpha$) 180° pulses during the HN(CO)CA-QJ (HNCO-QJ) experiments (cf., Figure 1) results in a fraction of $^{13}C^\alpha$ ($^{13}C'$) nuclei being modulated by $^1J_{C'C^\alpha}$ during t_1, thereby giving rise to a poorly resolved doublet that overlaps with the singlet resonance for which $^1J_{C'C^\alpha}$ has been removed. The same apparent lineshape anomaly will be observed for $^{13}C^\alpha$ in the HN(CO)CA-QJ experiment when the coupled $^{13}C^\beta$ spins are not inverted by the RE-BURP pulse. Since in the reference and attenuated spectra the unresolved doublet represents the same fraction of the superimposed singlet the cross-peak intensity ratio (and hence the extracted $^1J_{C'C^\alpha}$ value) is not affected. Using careful ^{13}C pulse width calibration, the distortions of the type described above were nearly invisible.

Second, we consider the effect of $^1J_{C'C^\alpha}$ evolution during the inversion and refocusing pulses on the extracted $^1J_{C'C^\alpha}$ value. Equation 4 assumes that $^1J_{C'C^\alpha}$ evolution takes place only during the delays between the 180° $^{13}C'$ and $^{13}C^\alpha$ pulses, but not during the pulses (which can occupy a significant fraction, between ca. 2 and 13%, of the 2T period). If transverse ^{13}C coherences are dephased by $^1J_{C'C^\alpha}$ for a combined additional time $2\delta t$ during the pulses (i.e., dephasing times of $2(T' - \Delta + \delta t)$ and $2(T' + \delta t)$ for the refer-

ence and attenuated spectra, respectively) the resulting I_{att}/I_{ref} ratio (ignoring the other potential sources of error discussed above) is given by Equation 7 with $\lambda = 1$ and $\varepsilon = -\sin(2\pi J T')\tan(2\pi J \delta t)$. Calculations indicate that for $\delta t = \kappa T'$ with $\kappa < 0.01$ (i.e., up to ~ 300 μs of additional $^1J_{C'C^\alpha}$ evolution for the 28 ms dephasing period) the systematic errors in $^1J_{C'C^\alpha}$ (isotropic) and $^1J_{C'C^\alpha} + {}^1D_{C'C^\alpha}$ (aligned) measurements almost completely cancel each other, yielding an accurate measurement of $^1D_{C'C^\alpha}$. For the pulses used in this work ($\sin x/x$, RE-BURP and hyperbolic secant), which have symmetric excitation profiles, the $^1J_{C'C^\alpha}$ evolution during the pulses is essentially fully refocused and can be neglected during the data analysis.

Conclusions

The quantitative J correlation methods described here can be used for the precise and accurate measurement of one-bond dipolar $^{13}C'$-$^{13}C^\alpha$ couplings in weakly aligned proteins with high resolution and sensitivity. We demonstrate for two systems, GB3 and αS in complex with a detergent micelle, that $^1D_{C'C^\alpha}$ can be determined with estimated uncertainties of ca. 0.2 Hz or better. For GB3 the measured dipolar couplings are in excellent agreement with the available high-resolution X-ray and NMR-refined structures, and the precision estimated for the couplings determined in αS represents a nearly two-fold improvement over the conventional $^{13}C^\alpha$-coupled HNCO measurements of $^1D_{C'C^\alpha}$. Notably, a very simple, single-parameter model was used to extract the value of $^1J_{C'C^\alpha}$ in the isotropic and aligned phases, and we have shown that for the accurate measurement $^1D_{C'C^\alpha}$, the effects of passive $^{13}C'$-$^{13}C^\alpha$ couplings, incomplete isotopic ^{13}C enrichment and nonideal inversion and refocusing ^{13}C pulses can typically be neglected for weakly aligned proteins. For high molecular weight $^2H,^{13}C,^{15}N$-labeled proteins the 3D TROSY-HN(CO)CA-QJ method offers the best results, while for $^{13}C,^{15}N$-labeled samples the 3D TROSY-HNCO-QJ experiment or a regular gradient- and sensitivity-enhanced HSQC version thereof is preferable; for systems with incomplete (< 90–95%) ^{13}C labeling the HN(CO)CA-QJ experiment or an HNCO-QJ method that includes a $^{13}C'$-$^{13}C^\alpha$ spin-pair filter should be used.

Supporting Information Available: One table containing the $^1D_{C'C^\alpha}$ values measured with three different pulse schemes for GB3; one table listing the $^1D_{C'C^\alpha}$ values measured in α-synuclein; one figure with the pulse sequence of the gradient-enhanced HSQC version of the HN(CO)CA-QJ experiment; one figure with the pulse sequence of the gradient-enhanced HSQC version of the HNCO-QJ experiment; two figures with pulse sequences for multiple-quantum-filtered versions of the 3D TROSY-HNCO-QJ experiment; three plots with pairwise correlations of $^1D_{C'C^\alpha}$ values measured in α-synuclein with three different methods. This material is available in the electronic edition of the journal at http://kluweronline.com/issn/0925-2738. Pulse sequence code for Bruker spectrometers can be found at http://spin.niddk.nih.gov/bax/

References

Annila, A., Aitio, H., Thulin, E. and Drakenberg, T. (1999) *J. Biomol. NMR*, **14**, 223–230.

Bax, A., Kontaxis, G. and Tjandra, N. (2001) *Meth. Enzymol.*, **339**, 127–174.

Bax, A., Vuister, G.W., Grzesiek, S., Delaglio, F., Wang, A.C., Tschudin, R. and Zhu, G. (1994) *Meth. Enzymol.*, **239**, 79–105.

Bryce, D.L. and Bax, A. (2004) *J. Biomol. NMR*, **28**, 273–287.

Chandra, S., Chen, X., Rizo, J., Jahn, R. and Sudhof, T.C. (2003) *J. Biol. Chem.*, **278**, 15313–15318.

Chou, J.J., Delaglio, F. and Bax, A. (2000) *J. Biomol. NMR*, **18**, 101–105.

Chou, J.J., Gaemers, S., Howder, B., Louis, J.M. and Bax, A. (2001) *J. Biomol. NMR*, **21**, 377–382.

Clore, G.M., Gronenborn, A.M. and Bax, A. (1998a) *J. Magn. Reson.*, **133**, 216–221.

Clore, G.M., Starich, M.R. and Gronenborn, A.M. (1998b) *J. Am. Chem. Soc.*, **120**, 10571–10572.

Clore, G.M., Starich, M.R., Bewley, C.A., Cai, M.L. and Kuszewski, J. (1999) *J. Am. Chem. Soc.*, **121**, 6513–6514.

Delaglio, F., Grzesiek, S., Vuister, G.W., Zhu, G., Pfeifer, J. and Bax, A. (1995) *J. Biomol. NMR*, **6**, 277–293.

Delaglio, F., Kontaxis, G. and Bax, A. (2000) *J. Am. Chem. Soc.*, **122**, 2142–2143.

Derrick, J.P. and Wigley, D.B. (1994) *J. Mol. Biol.*, **243**, 906–918.

Eliezer, D., Kutluay, E., Bussell Jr, R. and Browne, G. (2001) *J. Mol. Biol.*, **307**, 1061–1073.

Grzesiek, S. and Bax, A. (1992) *J. Magn. Reson.*, **96**, 432–440.

Grzesiek, S., Anglister, J., Ren, H. and Bax, A. (1993) *J. Am. Chem. Soc.*, **115**, 4639–4370.

Hall, J.B. and Fushman, D. (2003) *J. Biomol. NMR*, **27**, 261–275.

Hansen, M.R., Mueller, L. and Pardi, A. (1998) *Nat. Struct. Biol.*, **5**, 1065–1074.

Hu, J.-S. and Bax, A. (1997) *J. Am. Chem. Soc.*, **119**, 6360–6368.

Kay, L.E., Keifer, P. and Saarinen, T. (1992) *J. Am. Chem. Soc.*, **114**, 10663–10665.

Kontaxis, G., Clore, G.M. and Bax, A. (2000) *J. Magn. Reson.*, **143**, 184–196.

Losonczi, J.A., Andrec, M., Fischer, M.W.F. and Prestegard, J.H. (1999) *J. Magn. Reson.*, **138**, 334–342.

Ma, C. and Opella, S.J. (2000) *J. Magn. Reson.*, **146**, 381–384.

Meier, S., Häussinger, D. and Grzesiek, S. (2002) *J. Biomol. NMR*, **24**, 351–356.

Meiler, J., Blomberg, N., Nilges, M. and Griesinger, C. (2000) *J. Biomol. NMR*, **16**, 245–252.

Ottiger, M., Delaglio, F. and Bax, A. (1998) *J. Magn. Reson.*, **131**, 373–378.

Permi, P., Rosevear, P.R. and Annila, A. (2000) *J. Biomol. NMR*, **17**, 43–54.

Pervushin, K., Riek, R., Wider, G. and Wüthrich, K. (1997) *Proc. Natl. Acad. Sci. USA*, **94**, 12366–12371.

Pervushin, K., Wider, G. and Wüthrich, K. (1998) *J. Biomol. NMR*, **12**, 345–348.

Prestegard, J.H., Al-Hashimi, H.M. and Tolman, J.R. (2000) *Q. Rev. Biophys.*, **33**, 371–424.

Rückert, M. and Otting, G. (2000) *J. Am. Chem. Soc.*, **122**, 7793–7797.

Salzmann, M., Wider, G., Pervushin, K., Senn, H. and Wüthrich, K. (1999) *J. Am. Chem. Soc.*, **121**, 844–848.

Sass, H.J., Musco, G., Stahl, S.J., Wingfield, P.T. and Grzesiek, S. (2000) *J. Biomol. NMR*, **18**, 303–309.

Sørensen, M.D., Meissner, A. and Sørensen, O.W. (1997) *J. Biomol. NMR*, **10**, 181–186.

Tjandra, N. and Bax, A. (1997) *Science*, **278**, 1111–1114.

Tjandra, N., Omichinski, J.G., Gronenborn, A.M., Clore, G.M. and Bax, A. (1997) *Nat. Struct. Biol.*, **4**, 732–738.

Tolman, J.R., Flanagan, J.M., Kennedy, M.A. and Prestegard, J.H. (1995) *Proc. Natl. Acad. Sci. USA*, **92**, 9279–9283.

Tycko, R., Blanco, F.J. and Ishii, Y. (2000) *J. Am. Chem. Soc.*, **122**, 9340–9341.

Ulmer, T.S., Ramirez, B.E., Delaglio, F. and Bax, A. (2003) *J. Am. Chem. Soc.*, **125**, 9179–9191.

Vuister, G.W. and Bax, A. (1992) *J. Magn. Reson.*, **98**, 428–435.

Weigelt, J. (1998) *J. Am. Chem. Soc.*, **120**, 10778–10779.

Yamazaki, T., Lee, W., Arrowsmith, C.H., Muhandiram, D.R. and Kay, L.E. (1994) *J. Am. Chem. Soc.*, **116**, 11655–11666.

Yang, D., Venters, R.A., Mueller, G.A., Choy, W.Y. and Kay, L.E. (1999) *J. Biomol. NMR*, **14**, 333–343.

Supporting Information

Quantitative J correlation methods for the accurate measurement of $^{13}\text{C}'$-$^{13}\text{C}^{\alpha}$ dipolar couplings in proteins

Christopher P. Jaroniec, Tobias S. Ulmer and Ad Bax

Table S1. One-bond $^{13}C'$-$^{13}C^\alpha$ dipolar couplings measured in ^{13}C,^{15}N-labeled GB3, aligned in 10 mg/ml Pf1, using the 3D HN(CO)CA-QJ (Figure S1) and 3D HNCO-QJ (Figure S2) pulse schemes and from the F_1 doublets of a conventional $^{13}C^\alpha$-coupled 3D HNCO spectrum.

Residue	$^{13}C'$-$^{13}C^\alpha$ Dipolar Coupling, $^1D_{C'C^\alpha}$ (Hz)		
	HN(CO)CA-QJ	HNCO-QJ	HNCO F_1 doublets
M1	-0.43	-0.26	-0.36
Q2	2.79	3.05	3.07
Y3	-1.29	-1.24	-1.14
K4	3.92	3.99	3.91
L5	-1.42	-1.42	-1.45
V6	2.93	2.71	2.85
I7	-0.09	-0.03	-0.07
N8	2.11	2.14	2.19
G9	0.10	0.11	0.14
K10	-1.14	-1.04	-1.13
T11	3.86	3.83	4.27
L12	-1.57	-1.58	-1.57
K13	3.71	3.63	3.87
G14	-0.98	-0.96	-0.99
E15	0.46	0.49	0.49
T16	-0.93	-0.88	-0.82
T17	-1.67	-1.63	-1.58
T18	0.42	0.37	0.32
K19	-1.41	-1.39	-1.36
A20	-1.32	-1.32	-1.26
V21	0.25	0.24	0.20
D22	2.12	2.06	2.20
A23	0.52	0.47	0.52
E24	-1.75	-1.76	-1.78
T25	-1.66	-1.64	-1.79
A26	3.81	3.78	4.00
E27	-1.58	-1.72	-1.73
K28	-1.70	-1.59	-1.75
A29	0.07	0.09	0.15
F30	3.51	3.53	3.66
K31	-2.32	-2.11	-2.30
Q32	-1.90	-1.90	-1.97
Y33	2.80	2.75	2.84
A34	0.39	0.35	0.46
N35	-1.88	-1.85	-2.01
D36	-1.52	-1.58	-1.65
N37	3.49	3.59	3.69
G38	-1.63	-1.58	-1.63

V39	-1.16	-1.18	-1.21
D40	-1.31	-1.38	-1.41
G41	-1.87	-1.81	-1.91
V42	3.77	3.63	4.02
W43	-2.11	-2.06	-2.14
T44	4.05	4.09	4.53
Y45	-1.77	-1.80	-1.74
D46	3.37	3.37	3.49
D47	1.20	1.21	1.30
A48	-0.92	-0.90	-1.04
T49	-2.15	-2.18	-2.36
K50	-0.42	-0.45	-0.22
T51	3.19	3.11	3.28
F52	-0.58	-0.51	-0.53
T53	1.87	1.90	1.96
V54	0.02	0.01	0.05
T55	2.38	2.29	2.32

Table S2. One-bond $^{13}C'$-$^{13}C^{\alpha}$ dipolar couplings measured in $^2H,^{13}C,^{15}N$-labeled αS in complex with a sodium dodecyl sulfate micelle and aligned in a stretched polyacrylamide gel using 3D TROSY-HN(CO)CA-QJ and 3D TROSY-HNCO-QJ methods (Figure 1), a 3D TROSY-HNCO-QJ method which employs a ^{13}C-^{13}C multiple-quantum filter to compensate for incomplete ^{13}C enrichment (Figure S3A), and from the F_1 doublets of a conventional $^{13}C^{\alpha}$-coupled 3D HNCO spectrum.

| Residue	$^{13}C'$-$^{13}C^{\alpha}$ Dipolar Coupling, $^1D_{C'C^{\alpha}}$ (Hz)			
	HN(CO)CA-QJ	HNCO-QJ	HNCO-QJ MQ filtered	HNCO F_1 doublets
M1	—	—	—	—
D2	0.19	0.16	0.35	0.14
V3	-1.64	-1.53	-1.78	-1.71
F4	-0.18	-0.22	-0.18	-0.02
M5	-0.56	-0.32	-0.02	-0.35
K6	0.05	-0.04	-0.39	-0.33
G7	-1.85	-1.36	—	-2.37
L8	0.17	-0.07	0.55	-0.33
S9	-0.85	-0.72	-0.61	-0.66
K10	0.11	0.01	-0.16	-0.14
A11	-1.51	-1.29	-1.64	-2.15[a]
K12	-0.46	-0.68	-0.67	-0.68
E13	0.37	0.14	-0.09	0.47
G14	-0.79	—	—	—
V15	-0.97	-0.61	-0.76	-0.39
V16	-1.04	-0.96	-0.78	-1.34
A17	0.76	0.49	1.47	0.42
A18	-1.30	-1.61	-1.59	-1.69
A19	-0.99	-1.05	-1.48	-0.66
E20	-0.75	-0.60	-1.01	-0.38
K21	1.06	0.19	0.23	—[a]
T22	-0.81	—	—	-1.47[a]
K23	-1.53	-1.23	-1.78	-1.73
Q24	0.51	0.49	0.31	0.33[a]
G25	-0.11	—	—	-0.07[a]
V26	-1.12	-1.01	-1.17	-0.83
A27	-1.40	-1.14	-1.12	-1.10
E28	0.94	0.90	0.86	1.08
A29	-0.50	-0.32	-0.58	-0.31
A30	-1.38	-1.26	-1.38	-1.35
G31	-0.27	-0.36	-0.51	-0.07
K32	0.76	0.58	0.76	0.93
T33	-0.16	-0.17	-0.26	-0.54
K34	-0.95	-0.71	-0.96	-0.60
E35	0.58	0.43	0.54	-0.37

G36	0.05	0.00	0.19	-0.08
V37	-0.25	—	—	—[a]
L38	-0.11	—	—	—
Y39	-0.06	-0.06	0.30	-0.36
V40	—	—	—	—
G41	0.04	0.44	-0.78	-0.20
S42	-0.06	0.00	0.22	0.60
K43	0.27	0.42	0.09	—
T44	—	—	—	—
K45	0.99	0.99	1.54	1.08
E46	0.20	0.16	0.02	-0.10
G47	-1.69	-1.75	-2.42	-2.48
V48	0.13	0.18	0.45	0.14
V49	—	0.91	0.98	1.37
H50	-0.55	-0.37	-0.70	-0.23
G51	-1.77	-1.47	-1.36	-2.35
V52	0.68	1.11	1.18	1.55
A53	0.40	0.36	0.49	1.01
T54	-1.49	-1.36	-1.47	-1.45
V55	-1.23	-0.67	-0.62	-0.67
A56	1.43	1.18	1.07	1.12
E57	-0.08	0.31	-0.37	-0.16
K58	—	-2.19	-2.75	—
T59	-0.67	-0.15	-0.94	-0.29
K60	0.97	1.07	1.17	0.47
E61	-0.95	-0.74	-1.09	-1.36
Q62	-2.09	-1.76	-2.22	-2.78
V63	0.11	0.44	0.23	-1.03
T64	0.50	0.53	0.10	0.44
N65	-0.86	-0.76	0.01	-0.25
V66	-1.76	-1.55	-1.73	-1.37
G67	-1.31	-1.09	-1.00	-1.51
G68	-0.21	-0.33	-0.10	-1.07
A69	—	0.18	0.69	0.19
V70	-2.69	-2.57	-2.91	-3.73
V71	—	-0.41	0.28	—[a]
T72	0.78	0.78	0.42	0.01
G73	-0.30	-0.35	-0.73	-1.20
V74	-2.70	-2.78	-2.54	-3.14
T75	-0.11	-0.15	-0.76	-0.22
A76	0.42	0.69	-0.08	0.56
V77	-1.67	-1.41	-1.83	-1.95
A78	-1.94	-2.02	-2.33	-2.01
Q79	0.04	-0.09	0.14	0.50
K80	1.09	0.49	0.96	0.04[a]

T81	-2.65	—	—	—
V82	-1.23	-0.93	-1.10	-1.35
E83	0.86	0.81	0.82	1.18[a]
G84	0.90	0.75	0.72	0.78
A85	-3.09	-2.90	-3.06	-3.03
G86	1.69	1.73	1.75	1.83
S87	2.66	2.59	2.61	2.47
I88	-2.58	-2.34	-2.42	-2.48
A89	-1.19	-1.29	-0.88	-1.04
A90	2.29	2.39	2.04	2.21
A91	1.78	1.91	2.03	1.54
T92	-4.33	-3.50	-4.39	-3.72
G93	3.44	3.38	3.35	3.54
F94	-0.06	-0.11	-0.01	-0.07
V95	-0.31	-0.47	-0.56	-0.42
K96	-2.58	-2.53	-2.52	-2.94[a]
K97	-3.31	-3.00	-3.18	-3.56
D98	1.41	1.45	1.45	1.41
Q99	-1.41	-1.36	-1.46	-1.42
L100	-1.72	-1.66	-1.73	-1.63
G101	-1.19	-1.11	-1.12	-1.28
K102	-3.12	-2.83	-3.88	-3.44
N103	-2.64	-2.41	-2.55	-2.67
E104	-0.44	-0.45	-0.50	-0.62
E105	-1.61	-1.63	-1.82	-1.60
G106	-1.81	-1.82	-1.82	-2.01
A107	—	—	—	—
P108	-0.93	-0.86	-1.04	-0.76
Q109	-2.80	-2.75	-2.85	-3.27[a]
E110	-1.51	-1.74	-1.65	-1.80
G111	-1.27	-1.25	-1.39	-1.38
I112	-1.82	-1.77	-1.81	-1.88
L113	-1.73	-1.65	-1.74	-1.72
E114	-2.01	-2.02	-2.01	-2.03
D115	-0.96	-0.92	-0.98	-1.04
M116	—	—	—	—
P117	-1.08	-1.02	-1.07	-1.24
V118	-1.67	-1.62	-1.70	-1.85
D119	—	—	—	—
P120	-1.87	-1.80	-1.89	-1.86
D121	—	-0.55	-0.56	-0.42
N122	-0.90	-0.85	-0.85	-1.17
E123	-0.74	-0.76	-0.77	-0.76
A124	-0.62	-0.60	-0.62	-0.76
Y125	-1.20	-1.13	-1.21	-1.13

E126	-0.48	-0.50	-0.57	-0.56
M127	—	—	—	—
P128	-0.58	-0.51	-0.64	-0.60
S129	-0.75	-0.76	-0.77	-0.57
E130	-2.65	-2.80	-2.83	-3.28[a]
E131	-0.39	-0.42	-0.42	-0.17
G132	-0.35	-0.28	-0.40	-0.47
Y133	-0.23	-0.30	-0.20	-0.20
Q134	-0.36	-0.35	-0.28	-0.41
D135	-0.20	-0.27	-0.17	-0.13
Y136	-0.33	-0.31	-0.32	-0.40
E137	—	—	—	—
P138	-0.20	-0.18	-0.16	-0.17
E139	-0.07	-0.18	-0.14	-0.12
A140	—	—	—	—

[a] Partial overlap is observed between $^{13}C'$-$\{^{13}C^\alpha\}$ doublet components belonging to different residues in spectra recorded for isotropic and/or aligned samples.
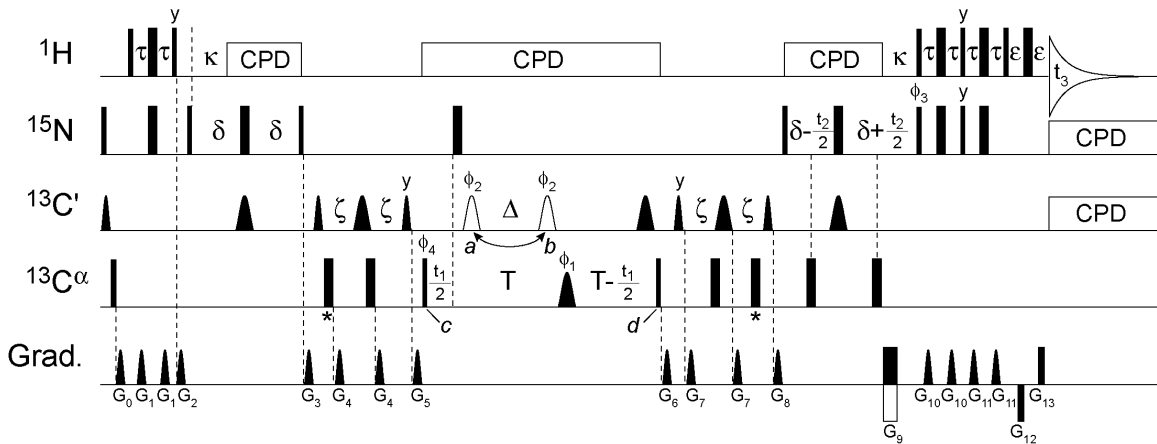
Figure S1. Pulse scheme of the gradient- and sensitivity-enhanced HSQC version of the 3D HN(CO)CA-QJ experiment. Narrow and wide pulses correspond to 90° and 180° flip angles (except for the open low-power 90° ^{1}H pulse), respectively. All pulses have phase x, unless indicated otherwise. The ^{1}H, ^{15}N, ^{13}C$'$, and ^{13}C$^\alpha$ carriers are positioned at 4.75 (water), 116, 177, and 56 ppm, respectively. ^{1}H pulses are applied at a field strength of 25 kHz, and a ^{15}N field of 5.3 kHz was employed. Composite pulse decoupling (CPD) is applied as follows: 2.5 kHz WALTZ-16 for ^{1}H, 1.1 kHz WALTZ-16 for ^{15}N, and 2.0 kHz GARP for ^{13}C$'$. The ^{13}C$^\alpha$ rectangular pulses are applied at field strengths of $\Delta\Omega/\sqrt{15}$ (90°) and $\Delta\Omega/\sqrt{3}$ (180°), where $\Delta\Omega$ is the frequency difference between the centers of the ^{13}C$'$ and ^{13}C$^\alpha$ chemical shift regions. All 90° and 180° ^{13}C$'$ shaped pulses have the profile of the center lobe of a sinx/x function, and durations of 75 μs and 150 μs, respectively (at 151 MHz ^{13}C frequency). The ^{13}C$^\alpha$ inversion pulses during the 2ζ periods are applied immediately following (first 2ζ period) and prior to (second 2ζ period) the ^{13}C$'$ pulses; the off-resonance effect (Bloch-Siegert) ^{13}C$^\alpha$ compensation pulses are denoted by asterisks. The 180° ^{13}C$^\alpha$ ϕ_1 pulse has the RE-BURP profile, duration of 400 μs (at 151 MHz ^{13}C frequency), and is centered at 45 ppm for the uniform inversion of the ^{13}C$^\alpha$ and ^{13}C$^\beta$ spins. Delay durations: τ = 2.35 ms, κ = 5.3 ms, δ = 12.5 ms, ζ = 4.3 ms, ε = 0.35 ms, $\Delta = T' = 14.0$ ms $\approx 3/(4^1J_{C'C^\alpha})$ (for the target value of $^1J_{C'C^\alpha} = 53.5$ Hz) and $T = T' + t_{180°}^N + t_{180°}^{C'} \approx 1/(2^1J_{C^\alpha C^\beta})$, where $t_{180°}^N$ and $t_{180°}^{C'}$ are the durations of the ^{15}N and ^{13}C$'$ 180° pulses, respectively. Phase cycling: $\phi_1 = x, y$; $\phi_2 = 2(x), 2(-x)$; $\phi_3 = x$; $\phi_4 = x$; receiver = $x, -x$. $^1J_{C'C^\alpha}$ dephasing takes place during the constant-time 2T period simultaneously with ^{13}C$^\alpha$ frequency labeling in t$_1$ (between time points c and d). Reference and attenuated spectra are acquired in an interleaved manner. For the reference spectrum the open ^{13}C$'$ pulse is applied in position a; for the attenuated spectrum in position b. States-TPPI phase cycling of ϕ_4 is used to obtain quadrature detection in the ^{13}C$^\alpha$ (F_1) dimension. Quadrature in the ^{15}N (F_2) dimension is achieved using the gradient- and sensitivity- enhanced method in which two data sets are recorded for each t_2 increment: one set with the pulse phases indicated above, and a second set with $\phi_3 = -x$ and the polarity of gradient G_9 inverted. The pulsed field gradients, sine-bell shaped with exception of G_9, G_{12} and G_{13} which are rectangular, are applied along the z-axis and have the following durations and strengths: $G_{0,1,2,3,4,5,6,7,8,9,10,11,12,13}$ = (2, 2, 4, 1, 2, 1, 1, 2, 1, 2.8, 2, 2, 0.180, 0.104 ms) and (3, 12, 24, 18, 15, 12, 9, 15, 24, 30, 18, 21, -30, 30 G/cm).
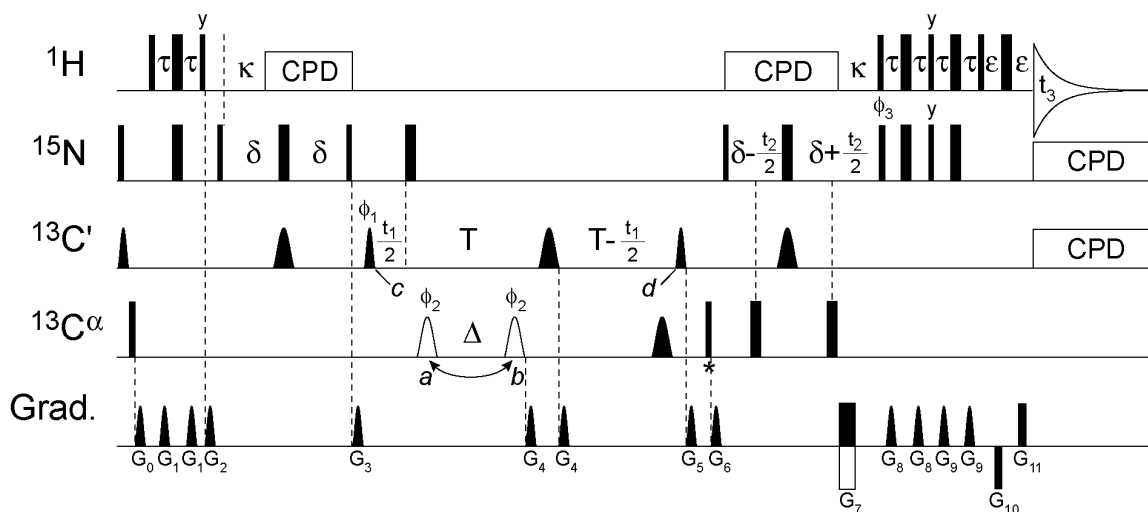
Figure S2. Pulse scheme of the gradient- and sensitivity-enhanced HSQC version of the 3D HNCO-QJ experiment. The majority of the experimental parameters are identical to those given in Figure S1 caption. The 180° $^{13}C^{\alpha}$ shaped pulses are of the hyperbolic secant type and have a squareness level, μ, of 6 and durations of 2 ms (at 151 MHz ^{13}C frequency). The 90° $^{13}C^{\alpha}$ pulse after the 2T period (denoted by an asterisk) suppresses minor E.COSY-like distortions of the cross-peaks in the F_3 dimension arising from the small fraction of $^{13}C'$ nuclei evolving under $^{1}J_{C'C^{\alpha}}$ during t_1, for which the coupled $^{13}C^{\alpha}$ is not inverted by the hyperbolic secant pulses. Delay durations: $\tau = 2.35$ ms, $\kappa = 5.3$ ms, $\delta = 12.5$ ms, $\zeta = 4.3$ ms, $\varepsilon = 0.35$ ms, $\Delta = T' = 14.0$ ms $\approx 3/(4^{1}J_{C'C^{\alpha}})$ and $T = T' + t^{N}_{180°} + t^{C^{\alpha}}_{180°} + t_G$, where $t^{N}_{180°}$, $t^{C^{\alpha}}_{180°}$ and t_G are the durations of the ^{15}N and $^{13}C^{\alpha}$ 180° pulses and gradient G_4, respectively. Phase cycling: $\phi_1 = x$, $-x$; $\phi_2 = 2(x)$, $2(-x)$; $\phi_3 = x$; receiver $= x$, $-x$. $^{1}J_{C'C^{\alpha}}$ dephasing takes place during the constant-time 2T period simultaneously with $^{13}C'$ frequency labeling in t_1 (between time points c and d). Reference and attenuated spectra are acquired in an interleaved manner. For the reference spectrum the open $^{13}C^{\alpha}$ pulse is applied in position a; for the attenuated spectrum in position b. States-TPPI phase cycling of ϕ_1 is used to obtain quadrature detection in the $^{13}C'$ (F_1) dimension. Quadrature in the ^{15}N (F_2) dimension is achieved using the gradient- and sensitivity-enhanced method described in the Figure S1 caption with the polarity of gradient G_7 inverted. The pulsed field gradients, sine-bell shaped with exception of G_7, G_{10} and G_{11} which are rectangular, are applied along the z-axis and have the following durations and strengths: $G_{0,1,2,3,4,5,6,7,8,9,10,11} = (2, 2, 4, 1, 0.5, 1, 1, 2.8, 2, 2, 0.180, 0.104$ ms) and $(3, 12, 24, 18, 15, 24, 9, 30, 18, 21, -30, 30$ G/cm).
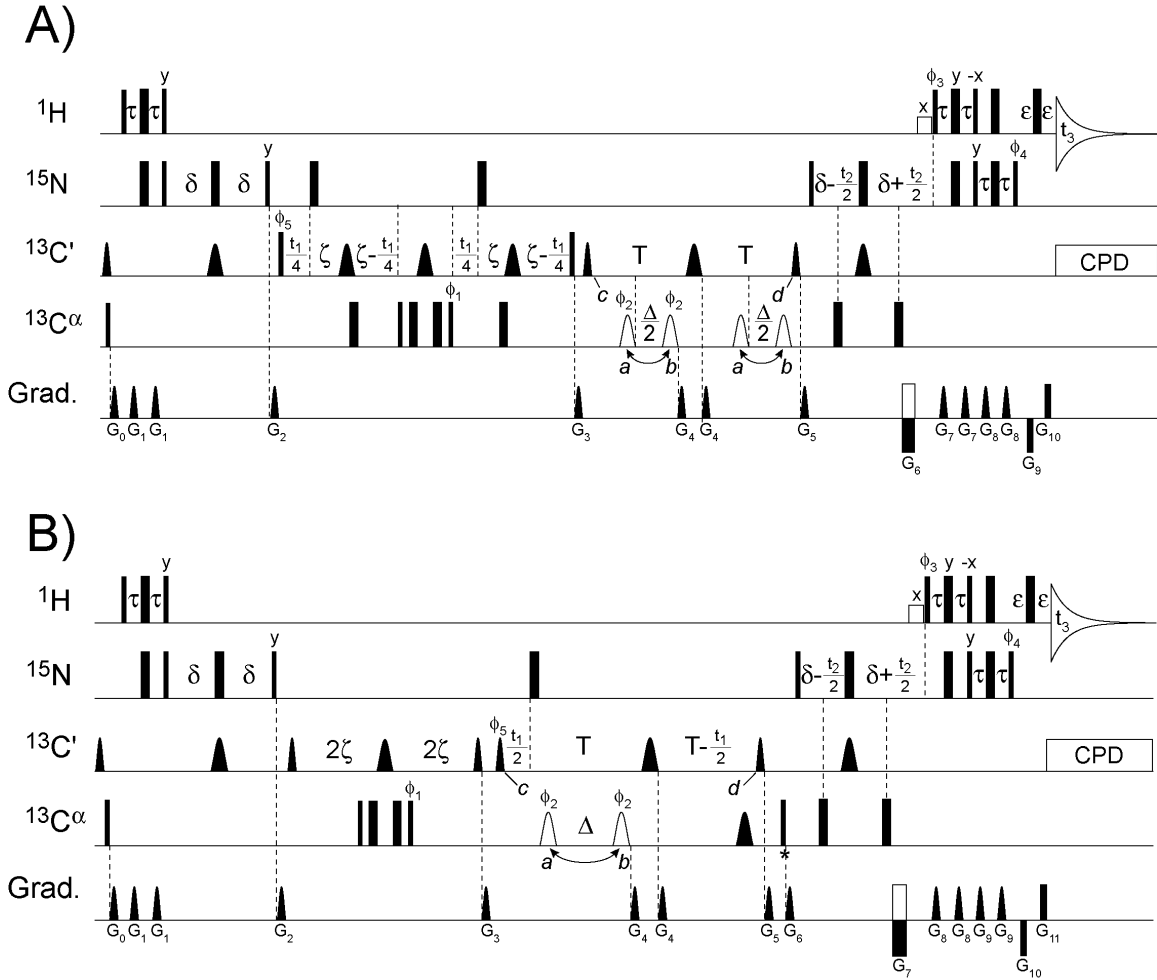
Figure S3. Pulse schemes of two 3D TROSY-HNCO-QJ experiments, which employ a $^{13}C'$-$^{13}C^\alpha$ multiple-quantum (MQ) spin-pair filter (during the 4ζ period preceding the $^1J_{C'C^\alpha}$ dephasing period 2T) to eliminate systematic errors in the measurement of $^1J_{C'C^\alpha}$ due to incomplete $^{13}C^\alpha$ labeling. The MQ filter removes the magnetization originating from $^{13}C'$ nuclei coupled to a $^{12}C^\alpha$ spin by alternating phase ϕ_1 in concert with the receiver. As described in the text the use of HNCO-QJ pulse schemes of this type, which have somewhat reduced sensitivity relative to the simple scheme of Figure 1B, will typically not be necessary for the accurate measurement of $^1D_{C'C^\alpha}$ in weakly aligned proteins with ^{13}C labeling efficiencies > ~95%. In (A) $^{13}C'$ frequency labeling is achieved in t_1, simultaneously with the MQ filter of total duration 4ζ (~17 ms), and in (B) $^{13}C'$ frequency labeling is achieved in t_1 simultaneously with the $^1J_{C'C^\alpha}$ dephasing period of duration 2T (~28 ms). We have used the 3D version of pulse scheme (A) to measure a nearly complete set of $^{13}C'$-$^{13}C^\alpha$ dipolar couplings in αS; these data are presented in Table S2 and Figure S4 and are in very good agreement with the quantitative $J_{C'C\alpha}$ measurements described in the text. In general however, pulse scheme (B) will be preferable since it affords equal sensitivity and superior resolution ($2T > 4\zeta$) compared to pulse scheme (A); in principle, the experiments could be further optimized to achieve simultaneous $^1J_{C'C^\alpha}$ dephasing and $^{13}C'$ frequency labeling in t_1, during the entire $2T+4\zeta$ period. The majority of the experimental parameters are identical to those

given in Figure S1 caption. The $^{13}C'$ rectangular pulses are applied at field strengths of $\Delta\Omega/\sqrt{15}$ (90°) and $\Delta\Omega/\sqrt{3}$ (180°), where $\Delta\Omega$ is the frequency difference between the centers of the $^{13}C'$ and $^{13}C^\alpha$ chemical shift regions. The 180° $^{13}C^\alpha$ shaped pulses are of the hyperbolic secant type and have a squareness level, μ, of 6 and durations of 2 ms (at 151 MHz ^{13}C frequency). For the MQ filter the $^{13}C^\alpha$ and $^{13}C'$ chemical shift evolution during the short delay between the $^{13}C^\alpha$ 90° pulses is refocused using a $^{13}C'$ $\sin x/x$ 180° pulse and two $^{13}C^\alpha$ rectangular 180° pulses (applied sequentially as shown in the figure). The quantitative $^1J_{C'C^\alpha}$ measurements are carried out during the subsequent 2T period (between time points c and d) as described below. Scheme (A): Delay durations: $\tau = 2.35$ ms, $\delta = 12.5$ ms, $\zeta = 4.3$ ms, $\varepsilon = 0.35$ ms, $\Delta = T' = 14.0$ ms $\approx 3/(4^1J_{C'C^\alpha})$ and $T = T' + t^{C^\alpha}_{180°} + t_G$, where $t^{C^\alpha}_{180°}$ is the length of the $^{13}C^\alpha$ 180° pulse, and t_G is the length of the gradient G_4. Phase cycling: $\phi_1 = x, -x$; $\phi_2 = 2(x), 2(-x)$; $\phi_3 = y$; $\phi_4 = x$; $\phi_5 = x$; receiver $= x, 2(-x), x$. Reference and attenuated spectra are acquired in an interleaved manner. For the reference spectrum the open $^{13}C^\alpha$ pulses are applied in positions a; for the attenuated spectrum in positions b. States-TPPI phase cycling of ϕ_5 is used to obtain quadrature detection in the $^{13}C'$ (F_1) dimension. Quadrature in the ^{15}N (F_2) dimension is achieved using the gradient- and sensitivity- enhanced method in which two data sets are recorded for each t_2 increment: one set with the pulse phases indicated above, and a second set with phases $\phi_3 = -y$ and $\phi_4 = -x$ and the polarity of gradient G_6 inverted. The pulsed field gradients, sine-bell shaped with exception of G_6, G_9 and G_{10} which are rectangular, are applied along the z-axis and have the following durations and strengths: $G_{0,1,2,3,4,5,6,7,8,9,10} = (2, 2, 1, 1, 0.5, 1, 2.8, 2, 2, 0.180, 0.104$ ms) and $(3, 12, 18, 12, 15, 24, -30, 18, 21, -30, 30$ G/cm). Scheme (B): The 90° $^{13}C^\alpha$ pulse after the 2T period (denoted by an asterisk) suppresses minor E.COSY-like distortions of the cross-peaks in the F_3 dimension arising from the small fraction of $^{13}C'$ nuclei evolving under $^1J_{C'C^\alpha}$ during t_1, for which the coupled $^{13}C^\alpha$ spin is not inverted by the hyperbolic secant pulses. Delay durations: $\tau = 2.35$ ms, $\delta = 12.5$ ms, $\zeta = 4.3$ ms, $\varepsilon = 0.35$ ms, $\Delta = T' = 14.0$ ms $\approx 3/(4^1J_{C'C^\alpha})$ and $T = T' + t^{N}_{180°} + t^{C^\alpha}_{180°} + t_G$, where $t^{N}_{180°}$, $t^{C^\alpha}_{180°}$ and t_G are the durations of the ^{15}N and $^{13}C^\alpha$ 180° pulses and gradient G_4, respectively. Phase cycling: $\phi_1 = x, -x$; $\phi_2 = 2(x), 2(-x)$; $\phi_3 = y$; $\phi_4 = x$; $\phi_5 = x$; receiver $= x, 2(-x), x$. Reference and attenuated spectra are acquired in an interleaved manner. For the reference spectrum the open $^{13}C^\alpha$ pulse is applied in position a; for the attenuated spectrum in position b. States-TPPI phase cycling of ϕ_5 is used to obtain quadrature detection in the $^{13}C'$ (F_1) dimension. Quadrature in the ^{15}N (F_2) dimension is achieved using the gradient- and sensitivity- enhanced method as described above with the polarity of gradient G_7 inverted. The pulsed field gradients, sine-bell shaped with exception of G_7, G_{10} and G_{11} which are rectangular, are applied along the z-axis and have the following durations and strengths: $G_{0,1,2,3,4,5,6,7,8,9,10,11} = (2, 2, 1, 1, 0.5, 1, 1, 2.8, 2, 2, 0.180, 0.104$ ms) and $(3, 12, 18, 12, 15, 24, 9, -30, 18, 21, -30, 30$ G/cm).
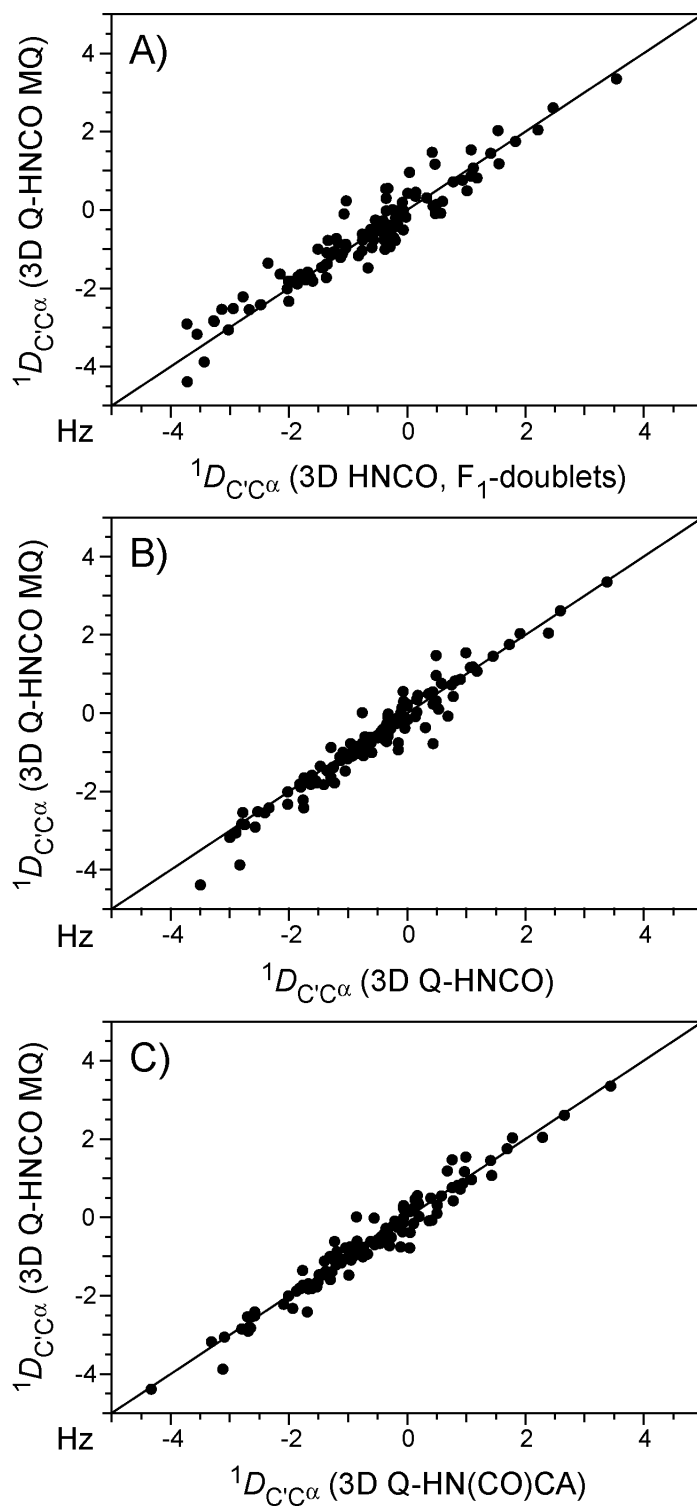
Figure S4. Plots of $^{13}C'$-$^{13}C^{\alpha}$ dipolar couplings, $^1D_{C'C^{\alpha}}$, measured in $^2H,^{13}C,^{15}N$-labeled αS in complex with an SDS micelle using the 3D TROSY-HNCO-QJ experiment, which employs a $^{13}C'$-$^{13}C^{\alpha}$ multiple-quantum (MQ) spin-pair filter to suppress errors in the measurement of $^1J_{C'C^{\alpha}}$ due to incomplete $^{13}C^{\alpha}$ labeling, and the pulse schemes described in the text. (A) $^1D_{C'C^{\alpha}}$ measured

from F_1 doublets of a conventional $^{13}C^\alpha$-coupled 3D TROSY-HNCO spectrum versus $^1D_{C'C^\alpha}$ from a 3D TROSY-HNCO-QJ MQ-filtered spectrum (pulse scheme of Figure S3A). (B) $^1D_{C'C^\alpha}$ measured from a 3D TROSY-HNCO-QJ spectrum (pulse scheme of Figure 1B) versus $^1D_{C'C^\alpha}$ from a 3D TROSY-HNCO-QJ MQ-filtered spectrum. (C) $^1D_{C'C^\alpha}$ measured from a 3D TROSY-HN(CO)CA-QJ spectrum (pulse scheme of Figure 1A) versus $^1D_{C'C^\alpha}$ from a 3D TROSY-HNCO-QJ MQ-filtered spectrum. The dipolar couplings are obtained as differences between $^1J_{C'C^\alpha}+^1D_{C'C^\alpha}$ and $^1J_{C'C^\alpha}$ values obtained by performing all experiments for the αS/micelle complex aligned in a stretched polyacrylamide gel and in the isotropic phase, respectively. The pairwise rms deviations for the structured residues 2-96 are 0.47 Hz for (A), 0.37 Hz for (B) and 0.32 Hz for (C); for all residues the rms deviations are 0.40 Hz for (A), 0.33 Hz for (B) and 0.28 Hz for (C).